ABSTRACT

PATIL NIKIL BABAN. Application of Vehicle Dynamics in Design and Development of an Autonomous Vehicle for EcoPRT. (Under the direction of Dr. Seth Hollar).

Majority of the automotive industry is investing heavily in the research of autonomous vehicles. EcoPRT (Economic Personal Rapid Transit) at NC State is a dedicated research group aspiring to reboot local transportation systems with the benefits and efficiency that autonomous technology has to offer, all with keeping the costs as low as possible. The prototype vehicles are designed and manufactured in-house by student teams and building a small, narrow track, and a lightweight vehicle that can hold two passengers is one of the key objectives of this project. The mechanical team is focused on streamlining the design and manufacturing process for the EcoPRT vehicles, and this thesis discusses the considerations and application of various design principles employed in the process. The work done in this thesis is twofold. The first part covers the design challenges imposed by narrow space and the modifications that were made to the previous designs to develop a custom independent suspension system. Significant emphasis has been given to the geometric parameter determination, kinematic analysis, and design calculations. The second part discusses the impact of the chosen design on various aspects of the vehicle's dynamic behavior. Attention is given to the rollover safety of the vehicle since it possesses a high risk of rollover for being narrow-tracked and relatively tall. Ride analysis is performed to study isolation behavior and compared to the previous design. Furthermore, the cornering stability of the vehicle is determined and compared with the previous model through understeer gradient analysis.

Application of Vehicle Dynamics in Design and Development of an Autonomous Vehicle for EcoPRT

by
Nikhil Baban Patil

A thesis submitted to the Graduate Faculty of
North Carolina State University
in partial fulfillment of the
requirements for the degree of
Master of Science

Mechanical Engineering

Raleigh, North Carolina

2017

APPROVED BY:

_____	_____
Dr. Seth Hollar Committee Co-chair	Dr. Paul Ro Committee Co-chair

_____

Dr. Andre Mazzoleni
Committee Member

DEDICATION

I dedicate this work to my parents and family for their never-ending support and belief in me,

my friends over here and overseas, whose company kept me going,

and the team of Triumphant Racers.

BIOGRAPHY

Nikhil was born and brought up in Mumbai, India. He graduated high school in 2009 in his hometown of Navi Mumbai. He went to college at the University of Mumbai and was conferred the undergraduate degree in Mechanical Engineering in 2013. He was the founding member of the FSAE chapter (Triumphant Racers) in his college and served as the design lead from the year 2011 till 2014. After graduating, he took a job at a startup where he spent one and a half year conducting seminars about automobile engineering and technologies and training and consulting college students to manufacture racecar prototype vehicles. Nikhil enrolled into the NC State University in the spring semester of 2016 for the Master's Degree. He has been working with EcoPRT since Summer 2016, leading the mechanical design team and building prototype vehicles.

ACKNOWLEDGEMENTS

I take this opportunity to appreciate Dr. Hollar and Marshal Brain for giving me the opportunity to be on their team. It has been an amazing year working with the team and have experienced a great many things. Dr. Hollar has always provided with valuable insights and Marshal with his cheerful visits time to time. I would also like to thank the student team working with me day and night to build the car. Working with Amit has been a great learning experience for me on the controls and electronics side. I would like to thank Brad for pushing the idea of redesigning the vehicle for safety and stability and working with me on the initial design of suspension. Moreover, I especially appreciate Joel for providing tremendous support throughout my tenure at the lab. I'd also like to mention Ben, Tyler, Maurice, Banu, Tim, Pushkar, Everett, Archika, and Ryan for all their help throughout the year. Finally, I appreciate our project sponsors NCDOT and the Research Triangle Park for supporting the EcoPRT research group. These research efforts and such an amazing work would not have been possible without their support.

TABLE OF CONTENTS

LIST OF TABLES

LIST OF FIGURES

LIST OF ABBREVIATIONS

a	Distance between CG and front axle
a_s	Distance between sprung mass CG and front axle
a_x, a_y	Longitudinal and Lateral acceleration
A_x, A_y	Longitudinal and Lateral acceleration in 'g'
b	Distance between CG and rear axle
b_s	Distance between sprung mass CG and rear axle
cpm	Cycles per minutes
C_f, C_r	Damping Coefficient
$C_{\alpha f}$, $C_{\alpha r}$	Cornering Stiffness
$C_{\gamma f}$, $C_{\gamma r}$	Camber Stiffness
E_{ff}, E_{fr}	Aligning torque deflection steer coefficients
FVSA	Front View Swing Arm
F	Force
F_{yr}, F_{yl}	Lateral Force
F_{zr}, F_{zl}	Normal Force
g	Acceleration due to gravity
h	CG height from ground
H	Distance between CG and Roll Axis
h2	Distance between sprung mass and Roll axis
hs	Sprung mass CG height from ground
I_B	Installation ratio of the ARB
IR	Installation ratio for the springs
K	Understeer gradient
K_s	Spring Rate
KPI	King Pin Inclination
K_{rr} K_{rf}	Spring rate of Front/Rear suspension
K_{sf}, K_{sr}	Front/Rear Spring rate
K_{wf}, K_{wr}	Front/Rear Wheel rate
K_t	Tire's spring rate
$K_{\theta Bf}$, $K_{\theta Br}$	Front /Rear ARB stiffness
$K_{\varphi Bf}$, $K_{\varphi Br}$	Front/Rear ARB applied stiffness
$K_{\varphi f}$, $K_{\varphi r}$	Front/Rear Suspension's roll stiffness
l	Wheelbase
LBJ	Lowe Ball Joint
LLT	Lateral Load Transfer
M, m	Mass
$N_{\alpha f}$, $N_{\alpha r}$	Aligning torque coefficients
r	Yaw rate
r_w	Wheel radius
R	Turn radius
RC	Roll Center
SPR	Side Pull Ratio
SSF	Static Stability Factor
SVSA	Side View Swing Arm
t	Trackwidth
t_f, t_r	Front and rear track width
TTR	Tilt Table Ratio
UBJ	Upper Ball Joint
V	Speed
w.r.t.	With respect to
W, W_t	Load (Total)
W_1, W_2	Load on front Left/Right wheels
W_3, W_4	Load on rear Left/Right wheels
W_f, W_r	Load on Front/Rear Wheels
W_s	Sprung load
W_{uf}, W_{ur}	Front/Rear Unsprung Load
x	Forward/Longitudinal direction
y	Side/Lateral direction
z	Vertical Direction
z_{rf}, z_{rr}	Front/Rear Roll Center heights
α	Angle of banking/slip angles
δ	Steering Angle
ε_f, ε_r	Roll steer coefficients.
θ	Grade
φ	Body/Frame roll angle
Γ_f, Γ_r	Roll Camber Coefficient
ω_f, ω_r	Front/Rear suspension frequency

CHAPTER 1: INTRODUCTION

1.1 Autonomous Vehicles

The invention of the automobile brought convenience and independence to the road transportation. The autonomous (driverless or self-driving) vehicles will potentially add to the mobility and safety factors facilitated by the current modes of transportation. An autonomous vehicle is capable of driving and navigating without any requirement of human input. These vehicles use a variety of sensors and actuators to sense the surroundings, plan appropriate paths, recognize traffic signs and signals, and maneuver around any obstacles.

Although the concept of autonomous vehicles has been around for decades, the first successful prototype autonomous vehicle is considered to be made by the Robotics Institute at Carnegie Mellon University in mid 80s. [1] The research team had developed a vision and control system for a robot that could drive down a road in continuous motion. Another early example is The Prometheus Project (1987-1995) which was the largest research and development program in the field of driverless cars at the time. Ernst Dickmanns and his team at Bundeswehr Universität München collaborating with Daimler-Benz developed two S-Class Mercedes cars (refer figure 1) that could drive on highways as well as heavy traffic without human intervention.

Currently, most of the auto-manufacturers that include GM, Ford, Mercedes, BMW, Audi, Volvo, Nissan, Toyota, and Tesla have invested heavily into the development of fully autonomous vehicles with some of the vehicles functional with partial autonomous driving conditions. A few of the recent notable developments in driverless vehicles is Tesla offering Autopilot function on its on-road vehicles for hands-free driving on highways and freeways, Uber has deployed a fleet of autonomous Ford vehicles in Pittsburgh (Sept 2017) and the Google Driverless Car (figure 1) that has logged 3 million miles driven by the fleet of its autonomous vehicles as of May 2017.

Figure 1. Mercedes VaMP (left) and Waymo/Google Car (right). (benzworld.org | waymo.com)

Considering the rapid movement in autonomous vehicle development, SAE International issued a report in 2014 [2] to define the classification of vehicles depending upon their level of autonomy (refer table 1). Complete automation of road vehicles will indicates increment the road safety by many folds. It should bring down the accidents caused by distracted or exhausted drivers or the late reaction times in case of emergency maneuvers. The road traffic could be more efficient as the speed limits can be increased and the space could be utilized more efficiently. It will enhance the mobility for the people with disabilities, elderly and even the young.

Table 1. Summary of SAE International's levels of driving automation for on-road vehicles.

SAE Level	Name	Narrative Definition	Execution of Steering And Acceleration/ Deceleration	Monitoring of Driving Environment	Fallback Performance of Dynamic Driving Task	System Capability (Driving Modes)
Human driver monitors the driving environment						
0	No Automation	The full-time performance by the human driver of all aspects of the dynamic driving task, even when enhanced by warning or intervention systems	Human driver	Human driver	Human driver	n/a
1	Driver Assistance	The driving mode-specific execution by a driver assistance system of either steering or acceleration/deceleration using information about the driving environment and with the expectation that the human driver performs all remaining aspects of the dynamic driving task	Human driver and system	Human driver	Human driver	Some driving modes
2	Partial Automation	The driving mode-specific execution by one or more driver assistance systems of both steering and acceleration/ deceleration using information about the driving environment and with the expectation that the human driver performs all remaining aspects of the dynamic driving task	System	Human driver	Human driver	Some driving modes
Automated driving system ("system") monitors the driving environment						
3	Conditional Automation	The driving mode-specific performance by an automated driving system of all aspects of the dynamic driving task with the expectation that the human driver will respond appropriately to a request to intervene	System	System	Human driver	Some driving modes
4	High Automation	The driving mode-specific performance by an automated driving system of all aspects of the dynamic driving task, even if a human driver does not respond appropriately to a request to intervene	System	System	Human driver	Some driving modes
5	Full Automation	The full-time performance by an automated driving system of all aspects of the dynamic driving task under all roadway and environmental conditions that can be managed by a human driver	System	System	System	All driving modes

1.2 Autonomous Vehicle Subsystems

A typical autonomous vehicle is equipped with the following systems to become completely operational.

1. Drive and actuation system
2. Navigation system
3. Perception system
4. Processing and control system

1.2.1 Drive and Actuation System

The drive system produces power required for accelerating or maintaining the speed of the vehicle. It may consist of an internal combustion engine or an electric motor drive with suitable drivetrain to deliver the power to the wheels. The brake and Steering actuators are incorporated to control the speed and direction of the vehicle.

1.2.2 Navigation System

The navigation system uses GPS satellite signals to identify the location of the vehicle. However, the GPS can only locate the vehicle to the accuracy of few meters. To achieve further accuracy, onboard systems such as Simultaneous Localization and Mapping (SLAM) algorithms, Inertial Measurement Units (IMU) and Odometery Systems are used.

1.2.3 Perception System

Perception system enables the vehicle to detect and identify the surroundings which could be utilized in various ways. The two subsystems of the perception system are Vision and Ranging. A stereo vision camera is used for image processing, object detection and identification, and depth perceptions. It can identify surroundings like vehicles, pedestrians, cyclists and map their distance from the vehicle. It can also identify road signs and signals. SLAM algorithms use stereo vision to identify the location of the vehicle and build the

environmental map. The ranging systems include Light Detection and Ranging (Lidar) and SONAR systems. Lidar utilizes laser pulse emitter and receiver to detect an object based on response time and it can be used more efficiently to map the surrounding environment without spending much of the processing power. On the other hand, SONAR systems are used to track the speeds of vehicles or other objects in the vehicle's vicinity.

1.2.4 Processing and Control System

The processing system is the command center of the vehicle. It handles all the control loops between sensors and actuators. This subsystem contains high powered processing units to analyze real-time data collected from vision and perception systems. This system is responsible for the decision making based on path planning and control algorithms that may include navigation, obstacle avoidance, object detection and identification, vehicle to vehicle communication, etc.

1.3 Personal Rapid Transit Systems

Personal Rapid Transit (PRT) is a mode of transport that consists of small capacity vehicles running on a network of guideways. The PRT system is similar to a light rail system except that passengers can board and travel on demand, it allows the point to point travel without any intermediate stops, ensuring no delay during the journey and making the nature of the transit truly personal even though it's public. A few examples of currently operational PRT systems as shown in figure 2, are 'UltraPRT' at Heathrow International Airport, UK, PRT at West Virginia University, Morgantown, US and '2getthere' at Masdar, UAE.

A PRT system can prove to be an efficient mode of transportation for a fast-growing city. The small size of vehicles requires reduces the size and thus the cost of infrastructure and the guideway network can be denser than that of a typical light rail system. The headway time of PRT can be significantly less than that of any conventional public transport utilizing the resources more efficiently.

Figure 2 Currently operational PRT Systems at Morgantown, West Virgina, US (left) and UltraPRT at Heathrow Airport, London, UK (right). (transportation.wvu.edu | ultraglobalprt.com)

1.4 EcoPRT at NC State

North Carolina State University at Raleigh is the largest public university in the state of North Carolina housing over 30000 students. The engineering schools are located either on the main campus or the Centennial Campus, and every day, thousands of students travel in between these two campuses to attend classes. The university provides free bus services – 'Wolfline' for the transit but the travel time compared to the travel distance is very high. The ever-growing population of students is set to burden the current transit even more and NC State has been exploring alternatives in its mobility plans. One of the solutions proposed according to the 2012 [3] report suggested utilizing a light rail system during peak hours of traffic. Given the costs of developments, the proposed plan has been put on hold. Meanwhile, the researchers at North Carolina State University are focused on solving the transportation problems faced by the university students and a fast-growing city like Raleigh.

In the year 2013, Dr. Seth Hollar and Marshal Brain suggested a cost-effective and efficient alternative to then proposed light rail system and the EcoPRT project was initiated. EcoPRT stands for Economic Personal Transit System. The project plans to establish a PRT system between the Main and the Centennial Campus of the university by connecting the D.

H. Hill and the James B. Hunt library which are the prime locations on each of the campus respectively.

Figure 3. The vision of EcoPRT. The pod-cars are imagined to be driving over roads, sidewalks or the elevated guideway.

EcoPRT is different from a typical PRT system. It aims to take advantage of both the elevated guideways and pre-existing pathways such as roads, sidewalks, and bike lanes (Figure 3) for transit. EcoPRT also oriented towards reducing the infrastructure costs significantly compared to the alternative systems. The goal for the cost of building an elevated guideway is to be approximately $1million/mile [4]. In this case, the size and weight of the vehicle become important factors of consideration.

1.5 Research Motivation of EcoPRT

Figure 4. The two generations of prototype vehicles built for EcoPRT. Generation 1 on the left and Generation 2 on the right.

Researchers at EcoPRT are actively working towards a pilot that will demonstrate the use of existing pathways for EcoPRT transit on the NC State campus. To date, two prototype vehicles have been built (Figure 4) and are undergoing on-road tests. Four additional vehicles have been planned to be manufactured for the on-campus pilot. The guiding principles for this research have been conceptualized [4] as follows:

1. Reduce costs related to infrastructure development compared to those needed for existing transit modalities like Bus Rapid Transit and Light Rail.
2. As simple and easy installation procedure as required putting in utility poles for a power line.
3. Adaptable installation with narrow guideway footprint and elevated guideway placement so that guideways may be installed nearly anywhere, including shoulders, medians, easements, greenways, sidewalks, etc.
4. Minimize travel time by ensuring no waiting at stations and no delays on the way for passengers
5. Reduce carbon footprint compared to any other widely operational transit modality.

6. Reduction in payload and labor cost by utilizing self-driving vehicles.

These guidelines direct the researchers at EcoPRT towards definite goals related to different aspects of the project. Emphasis has been given to matching the federal and industrial standards while developing the prototypes. Following are the key guidelines that shape the design orientation of the prototype vehicles.

1.5.1 Small and Narrow Footprint Vehicles

The average occupancy of cars in the US according to the National Household Travel Survey is 1.55 (figure 5). Thus, it was decided to make a two-passenger vehicle ensuring small size. The seating arrangement was made 'face to face' longitudinally to keep the footprint narrow which in result will require smaller guideways. A narrow and relatively tall vehicle would demand extensive stability in cornering and quick maneuvering. The design of suspension and steering revolves around making the ride as stable and comfortable as possible for the passengers.

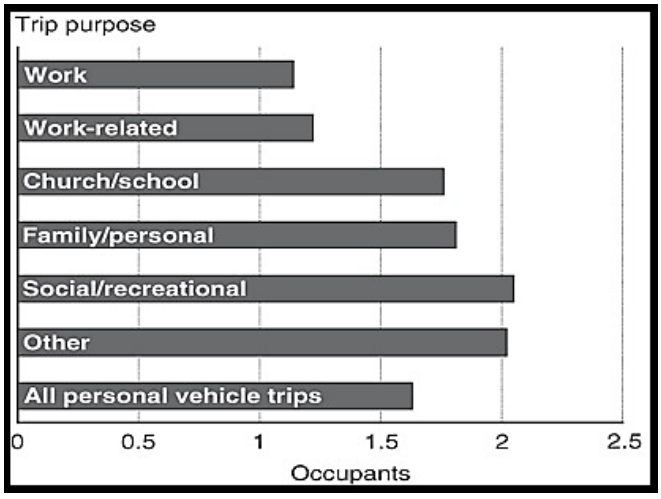

Figure 5 Average occupancy per vehicle for different trip purposes. (The 2001 National Household Travel Survey, daily trip file, U.S. Department of Transportation).

1.5.2 Low Cost

The EcoPRT vehicles are expected to cost approximately $10000 per unit. The low cost would yield reduced fares for passengers and ensure development and growth

opportunities for even small communities. The small size of the vehicle contributes heavily towards keeping the costs low. However, the sensors required for autonomy are usually expensive. EcoPRT has developed a low-cost 3D perception unit using LIDAR sensors that cost under $1500 [4]. Regarding mechanical design, the cost is kept low by opting for the parts that are available ‘on the shelf,' utilizing a ‘2 line-symmetrical’ structure and optimizing the design for low weight. The structural design is also aimed to be safe in case of mild impacts and rollovers (20-30mph).

1.5.3 Autonomous Functioning

EcoPRT would redefine the convenience of short-distance traveling. It aims to solve the problems faced by passengers traveling for short-distance (10 miles or less) with existing transit facilities. The vehicles need to utilize elevated guideways for faster transit and be able to navigate through existing roads and pathways. A vast amount of research is ongoing at EcoPRT to develop a control system for the autonomous functioning of multiple vehicles.

1.6 Thesis Outline

The objective of this thesis is to establish a design process and provide benchmark parameters for future vehicle development programs within EcoPRT.

Chapter 1 is the introduction to generic autonomous vehicles and their history. Basic subsystems involved in the control of an autonomous vehicle are discussed and the levels of autonomy as defined by SAE are described. This chapter also introduces the concept of Personal Rapid Transit Systems, the idea behind EcoPRT, and the research motivation. Chapter 2 describes the design background with introduction to the design facilitated by the previous generation model and the new design ideologies.

Chapter 3 defines the initial parameters and goals to be achieved by the final designs and the kinematic relationships of wheel alignments with respect to bump and roll motion are established. Chapter 4 deals with the rollover stability analysis by means of rollover threshold metrics. The chapter describes a steady state suspended vehicle model to determine actual rollover threshold which is thereafter utilized to determine the ride and roll rates of the vehicle. Furthermore, the chapter consists of a basic quarter car model analysis to compare the ride response of the previous and the new suspension designs.

Chapter 5 describes a steady state yaw plane bicycle model to establish the stability factor 'K' or the understeer gradient. It briefly discusses the contribution of kinematic relationships to the understeer gradient. Moreover, the work that needs to be done in near future has also been discussed.

CHAPTER 2: DESIGN BACKGROUND

2.1 Suspension and Steering

The suspension system of a vehicle consists of mechanical links with pivotal joints, springs, and dampers that keep the vehicle's frame suspended over the wheels. The suspension is also responsible for isolating the vehicle from road vibrations and bumps and keeping the passengers comfortable. The suspension also defines the road-holding characteristics of the vehicle by constraining the relative motion between the wheels and chassis. According to Gillespie [5], following are the primary functions of a suspension system.

1. Isolate the frame from road roughness and bumps by allowing vertical compliance.
2. Maintain the desired wheel alignment of the wheel in all conditions.
3. Provide resistance against body roll in lateral or pitching in longitudinal acceleration.
4. Keep the tire in contact with the road as much as possible with minimal variation in load.
5. React appropriately to the longitudinal/lateral control forces, and braking/driving torques.

The steering system is responsible for the directional control of the vehicle. It is important to design the steering linkage in a way that results in a stable response and minimal tire wear. Usually, vehicles are steered by the front wheels, but four-wheel steering can also be implied for additional maneuvering conditions. This chapter will discuss the type of the suspension and steering geometries utilized on both the generations and the thought process behind their setup.

2.2 Suspension Kinematics

The dynamic behavior of the vehicle mainly depends upon the kinematic properties of the suspension. Thus, it is essential to study the kinematic relationships of the suspension and steering linkage. It is critical to understand the tire performance and behavior to achieve

optimum dynamic performance out of the vehicle. The tire's performance depends heavily upon its alignment (Camber, Toe, Trail, Scrub). The suspension needs to be designed in such a way that the change in alignment of the wheel is kept in control. In case of the steering kinematics, the relationship between either of the steered wheels is defined by 'Ackerman Geometry.' It is another variation of 4-bar linkage that allows the inside wheel to be turned more than the outside wheel during cornering. Due to multibody geometries (usually in independent suspension), designing a perfect Ackerman geometry is not possible. Thus, the designs are chosen to have as close behavior as possible to perfect Ackerman. The following sections will discuss the suspension and steering setups in detail.

2.2.2 Gen 2 Suspension

The Gen 1 vehicle hosted rigid suspension with the brakes integrated only on the rear axle, a steel framework, and transparent polycarbonate body panels. The team decided to upgrade the Gen 2 vehicle with suspension, electro-hydraulic brakes, roll cage and aesthetic body panels. For simplicity, the team utilized parallel four-bar suspension (Figure 6) with Panhard bar for both front and rear axles. The front axle can be seen connecting the two wheels by a central beam that suspends the front side of the frame with two upright coilovers and the four links trail the axle longitudinally to connect with the frame. The steering actuator is connected between the axle and one of the wheels. The rear axle has a similar setup with the only difference being that the I place of the dead axle, the wheels are connected to a differential unit and half-shafts.

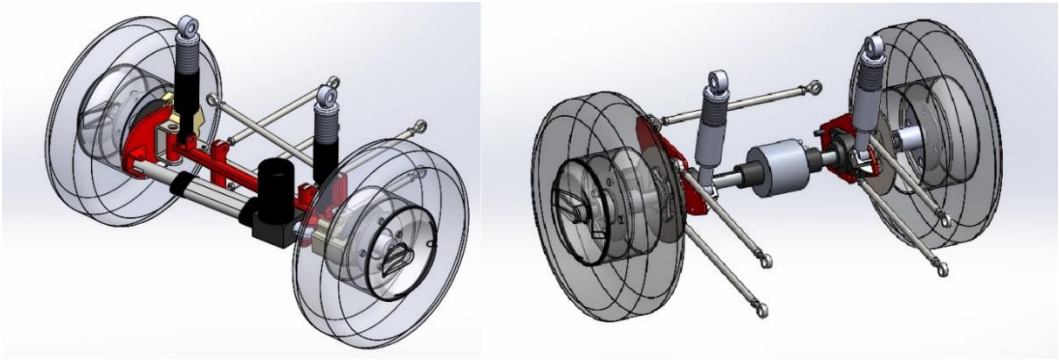

Figure 6. The four-bar suspension on the front (left) and rear (right) axles of Gen 2 Vehicle.

2.2.2 Gen 2.5 Suspension

As the Gen 2 vehicle was still in build-up process, the team decided to reassess the choice of suspension and the overall structure of the vehicle. One of the major observations was that the roll stiffness of the suspension was very low and that integration of the components was not space-efficient. The frame's structure also needed to be redesigned to add rigidity. Thus the team decided to redesign the suspension and chassis for the next vehicle (Gen 2.5).

The first choice of the suspension was 'McPherson Strut' for its simple integration and space efficiency. However, no suitably sized struts were available in the market, and the team decided against utilizing its resources to custom build a strut. Another major setback was to find a differential-half shaft assembly for a wheeltrack of 30.5 inches. The smallest differential was about 7-8 inches wide (Drexler, Torsen, etc.) and the shortest half shaft with CV joints on both ends was still 9 inches long. Ultimately it was decided to employ hub motors on both the rear wheels which would eliminate the entire drivetrain system and was easy to integrate. For the suspension geometry, the team decided upon using Short-Long-Arm (SLA) double wishbone suspension. In this geometry, wheel spindles are supported by an upper and lower 'A' shaped arm (Figure 7). The SLA would bring in the following advantages to the vehicle's design.

1. This geometry can tailor the kinematics of the suspension system for desired performance. (wheel alignment, tire contact, etc.)
2. There's room for minor modifications and further development without causing major changes. Considering the current phase of the ecoPRT project, this feature is essential.
3. The space efficiency is better than four-bar beam axle suspension allowing room for additional components.

A sway bar or anti-roll bar or stabilizer bar is also integrated with the SLA suspension that helps reduce the body roll of the vehicle during fast cornering. It connects opposite (left/right) wheels through short lever arms linked by a torsion beam. A sway bar increases the

suspension's roll stiffness—its resistance to roll in turns, in addition to the roll stiffness provided by the suspension springs. The anti-roll bar does not cause any effect in case of parallel wheel travel (both wheels traveling in unison in the vertical direction).

Figure 7. Double wishbone SLA suspension on gen 2.5 vehicle on the front (left) and the rear axle (right).

2.2.3 Gen 2 Steering

The steering system of Gen 2 vehicle utilizes a 6-inch motorized linear actuator placed in front of the axle that swings the right wheel (Figure 8). The left wheel is linked to the right wheel by means of a track rod behind the axle. The setup resembles a simple four-link Pro-Ackerman geometry with inside wheel having larger toe angle than the outside one.

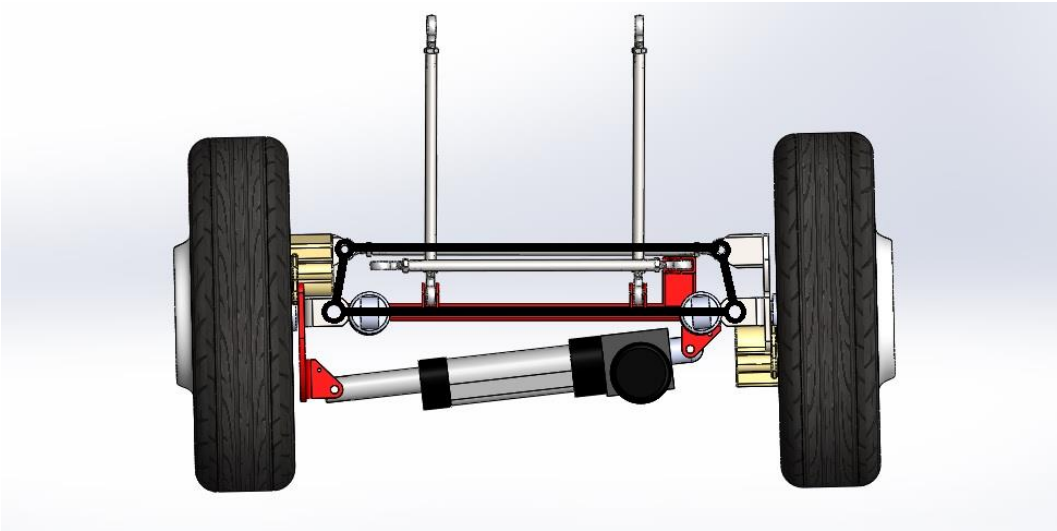

Figure 8. Gen 2 steering system linkage with a linear actuator and track road.

The issue with Gen 2 steering set-up is the large scrub radius. Which results in much resistance on the steering actuator and slows down the motion. The large scrub radius also causes the wheels to achieve a steer-angle (38^0) smaller than required (45^0).

2.2.4 Gen 2.5 Steering

As the suspension geometry was subject to change, the steering geometry had to be modified to suit the independent wheel movement. The gen 2.5 steering system is also Pro-Ackerman and utilizes motorized rack and pinion setup (Figure 9). The new geometry is designed to allow 45^0 toe at the inside wheel. The wheel knuckles are attached to a steering arm that is connected to the rack through tie rods. A linear potentiometer is added in parallel to the rack for feedback data. FEA analysis was performed on all the components for static and fatigue loading to ensure longevity.

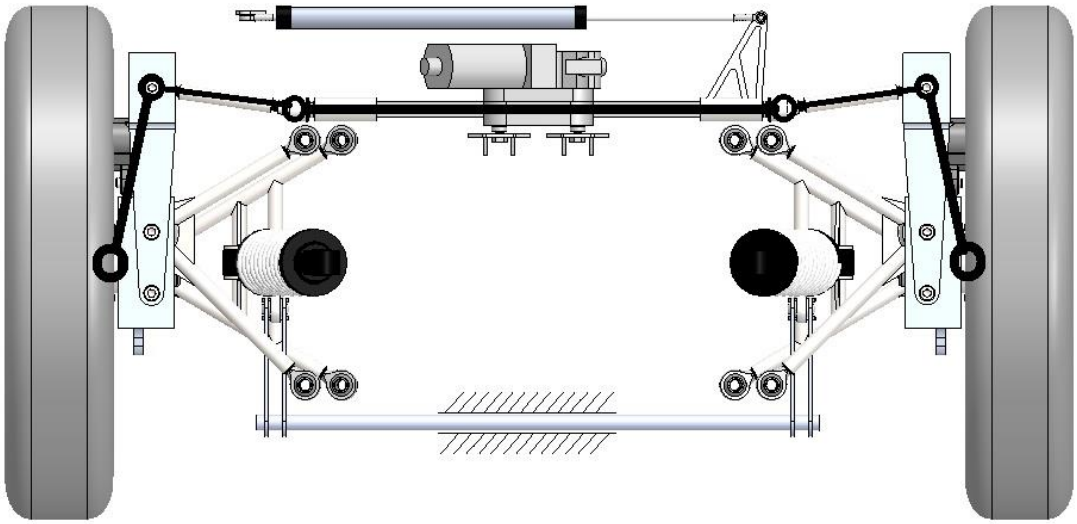

Figure 9. Gen 2.5 steering system linkage with a linear actuator and tie rods.

CHAPTER 3: KINEMATIC ANALYSIS

This chapter will discuss the step by step process of suspension design and parameter calculations. First, a collection of hardpoints is selected, and feasibility analysis is done using CAD software to verify that the geometry can be applied and all the suspension components can be integrated. After the feasibility check, multibody analysis software ADAMS was used to refine the geometry to achieve required results. The calculation procedures used in this chapter follow the references given in Milliken [6] and Dukkipati [7].

3.1 Initial Parameters and Constraints

To design the suspension system, Milliken [6] suggests a "wheel to frame' approach. Before one could start, a few parameters and requirements need to be decided. The parameters depend upon the type of vehicle one is building and the kind of environment it will be operated in. As per the demands of the project EcoPRT in current state, according to 49 CFR 571.500 - STANDARD NO. 500 of Federal Motor Vehicle Safety Standards, all the prototypes distinguish as Low-Speed Vehicles (LSV). The maximum speed that the EcoPRT prototype vehicles are required to achieve is 25mph. The vehicle weighs about 500lbs (Kerb weight) and should be able to carry a payload of 500lbs (Gross weight will be 1000 lbs). The gen 2 prototype gave an approximation for the location of CG and the weight distribution.

Table 2. Gen 2.5 suspension parameters and desired kinematic performance ranges.

Parameter	**Value or Range (Unit)**	**Parameter**	**Value or Range (Unit)**
Wheelbase	1.778 (70 inches)	Camber Change w.r.t. bump	<3º @ 0º static value
Wheeltrack	0.771 m (30.4 inches)	Toe Change w.r.t. bump	<2º @ 0º static value
Wheels	10 – 3.5	Damper/Spring Travel	±30.5 mm
Wheel travel	±50.8 mm	Half Track Change	±15 mm
KPI	<8º	Toe (steering)	45° for the inside tire
Caster	<8º	Turning Radius	<2500 mm
Zrc	>0mm @ max droop	Roll Gradient	<8.5°/g
Scrub Radius	As low as possible	Natural Ride Frequencies	≈ 2 Hz

3.2 Suspension Hardpoints

While designing the outboard pickup points, it is critical to be familiar with the components that are going to be integrated with the wheel hub and the knuckle. The first location to choose for is the Lower Ball Joint (LBJ). This location is important particularly with respect to the scrub radius, and then the Upper Ball Joint (UBJ) position with some King Pin Inclination (KPI) angle (Figure xx). The axis formed by the UBJ and LBJ is the wheel axis and the wheel swings about the pivots formed by these two joints when steered. The wheel axis also determines the mechanical trail formed due to caster angle which is a result of longitudinal offset between LBJ and UBJ.

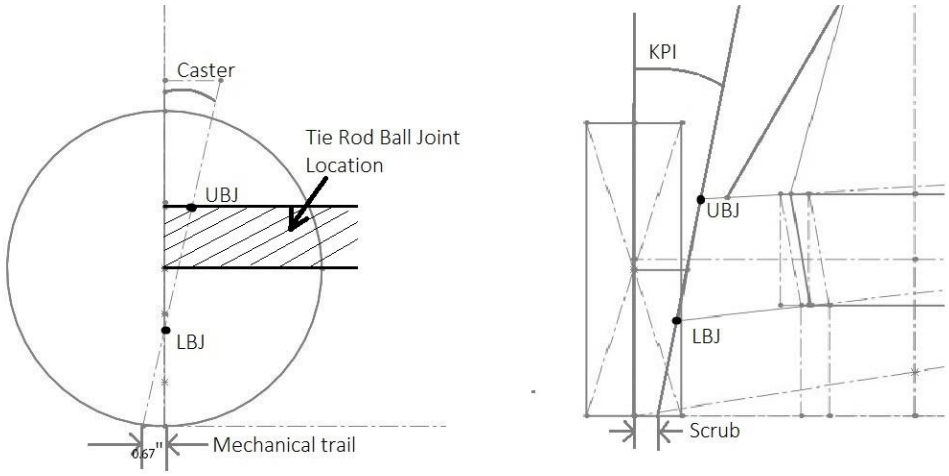

Figure 10. Determination of outboard pick-up points.

The inboard ball joint locations are decided next. These locations define the Front View Swing axle (FVSA) and Side View Swing Axle (SVSA) geometrically (Figure 11). The swing axles define the instant center of rotation for a wheel in respective plane of view. The larger the FVSA, smaller the change in Wheel Camber. FVSA also defines the static location of the Roll Center (RC) and its height from the ground height (z_{rc}). The roll center location has twofold effects on the dynamics of the vehicles. It determines two moment arms during lateral motion of the vehicle. The first one is regarding the roll moment and the second one is jacking forces. The closer the RC to the CG, smaller the roll moment. While on the other hand, closer the RC to the ground, smaller the jacking forces. Roll moment causes the body roll which could

result in instability in cornering and the jacking forces. It was decided to go with low RC and counter the roll moments with the aid of anti-roll bars. As the body travels in downward direction with respect to the wheels, the RC moves down as well. Thus, there is a minimum height consideration above which the RC should be located to compensate for the wheel jounce. The geometry selected for Gen 2.5 suspension has a horizontal SVSA, thus, Anti-dive and Anti-squat geometry considerations are not being taken into account.

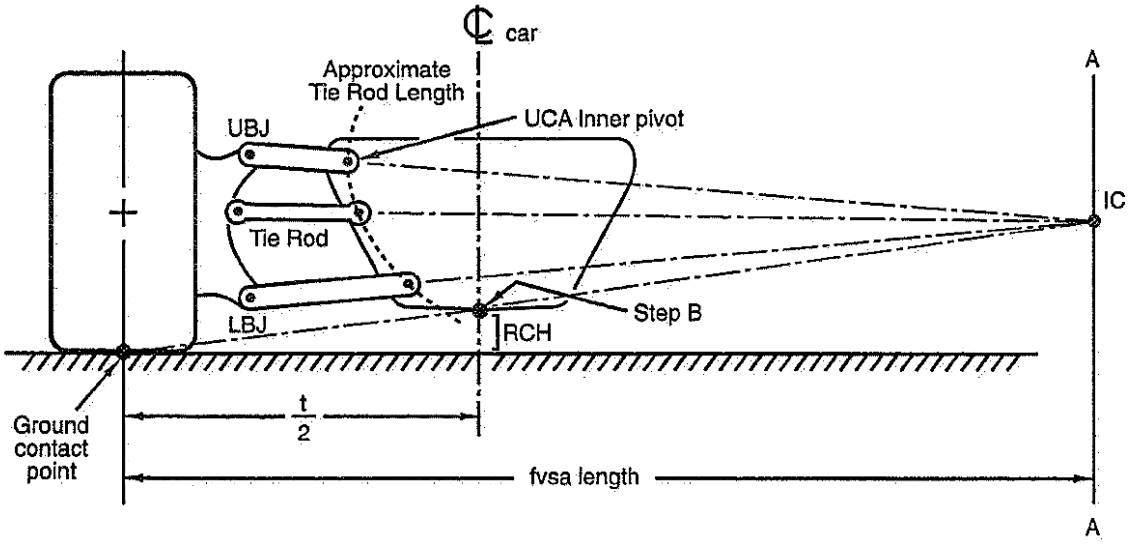

Figure 11. SLA front view geometry and swing axle length. (Milliken).

For the side-view geometry, the KPI is kept at 5^0. Considering the desired scrub radius, the Lower Ball Joint (LBJ) was kept as outwards as possible after making sure that enough room is left for the wheel assembly components like brake rotor, caliper and wheel bearings. Considering the front suspension geometry selected so far, the roll camber can be defined. The roll camber is the change in wheel camber compared to the change in body roll.

$$Roll\ Camber = \frac{Wheel\ Camber\ Angle}{Chassis\ Roll\ Angle\ (\Phi)} \tag{3.1}$$

And,

$$FVSA\ length = \frac{t}{2}(1 - Roll\ Camber) \tag{3.2}$$

Thus, combining eq. 3.1 and 3.2 we get,

$$Wheel\ Camber\ Angle = \Phi(1 - \frac{t}{2\ FVSA}) \qquad (3.3)$$

With FVSA length 1.868m and trackwidth (t) 0.771m and the maximum desired body roll 4 – 5^0, the wheel camber according to equation 3.3 comes out to be

$$Wheel\ Camber\ Angle = 5\ (1 - \frac{0.771}{2\ x\ 1.868}) = \mathbf{3.9^0}$$

The camber angle found above is the gain in wheel camber during the body roll and the suspension geometry should try to compensate for this gain by reducing the wheel camber in bump. The outboard points were defined at the wheel by considering the wheel offset, the space available inside the rim and desired KPI. The inboard points were chosen depending upon the minimum required ground clearance, FVSA length and the camber gain obtained by simulating the wheel in bump and rebound in 2D geometry (figure 12). The Coilover mounting points were chosen depending upon the maximum height of the upper mounting which had to be below the passenger seat and the lower mounting had to be as much inside that the spring would not intrude with the hub motor's wire outlet.

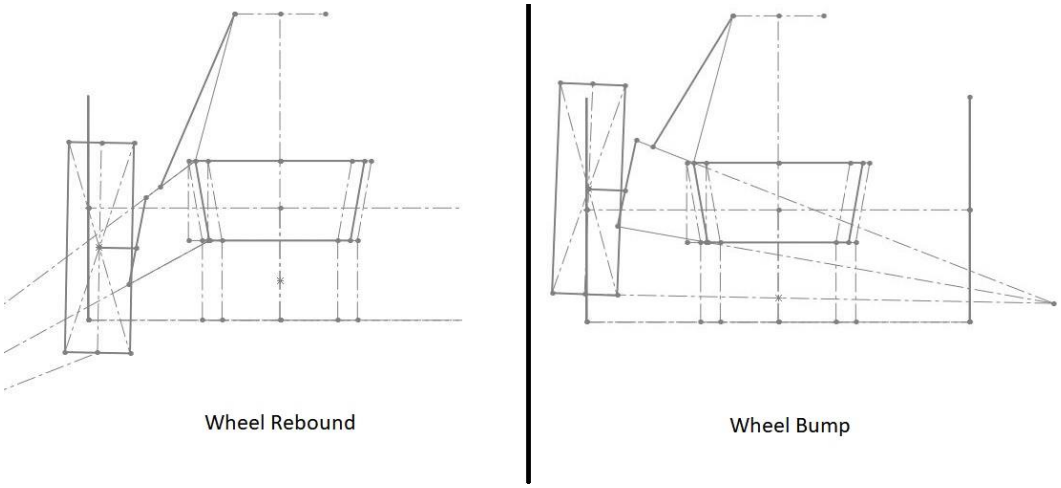

Figure 12. Preliminary 2D Kinematic simulation in Solidworks sketch.

The steering geometry mainly involves deciding the position of the inner and the outer ball joint of the tie rod. The Ackerman geometry, as mentioned before, cannot be perfect, but it is possible to achieve a close performance. The objectives of the steering system are as follows.

1. Achieve required toe difference for 45 degrees turning capability (for inside wheel).
2. Achieve as small toe- change as possible in bump/droop.

A few iterations were done in Solidworks sketcher until suitable geometry was found (table 3).

Table 3. Finalized suspension hardpoints.

Front Axle		**Lateral**	**Longitudinal**	**Vertical**
	Center	385.55	0	207.01
Wheel	Ground Contact	385.55	0	0
	Upper Ball Joint	316.43	-25	282.01
Upright	Lower Ball Joint	329.55	0	132.01
	Upper Fore	190.55	100	290
	Upper Aft	190.55	-100	290
	Lower Fore	160.55	100	156.35
Control Arm	Lower Aft	160.55	-100	156.35
	Lower	254.97	0	139.95
Coilover	Upper	177.13	0	474
	Tie Rod Outboard	315.92	-142.8	308.82
Tie Rod	Tie Rod Inboard	196.85	-125	315.4
Rear Axle				
	Center	385.55	-1778	207.01
Wheel	Ground Contact	385.55	-1778	0
	Upper Ball Joint	253.47	-1803	282.01
Upright	Lower Ball Joint	266.59	-1778	132.01
	Upper Fore	127.59	-1678	290
	Upper Aft	127.59	-1878	290
	Lower Fore	97.59	-1678	156.35
Control Arm	Lower Aft	97.59	-1878	156.35
	Lower	191.59	-1778	139.95
Coilover	Upper	114.17	-1778	474
	Outboard	253.47	-1753	282.01
Toe Link	Inboard	127.59	-1678	290

3.3 Kinematic Analysis

The principal motive for redesigning the Gen 2 vehicle was to add stability and comfort by changing the suspension from dependent to independent. As the wheels can move independent of each other, unlike dependent suspension, they undergo change in alignment. These variations are constrained by the geometry of the linkage and can be tailored to achieve desired performance. This study is performed to understand the kinematic behavior of the wheels when subjected to a constrained motion. The kinematic analysis was done using ADAMS multibody dynamic simulation platform (figure 13). The alignments that this study is interested in are as follows.

1. Camber: Camber is the angle made by the wheel's centerline with vertical when viewed from the front. A wheel could have static camber and it is also subject to change as the wheel moves up and down w.r.t. the frame, as it swings about its instant center defined by the suspension geometry.
2. Scrub: The Lateral movement of the wheel as it moves up and down w.r.t. the frame is called as Scrub. As the wheel undergoes scrub, the wheeltrack changes and it could affect the stability of the vehicle. It also causes tire wear, as the contact patch rubs against the road surface.
3. Toe: The inclination of the wheel with the longitudinal plane when vied from the top is known as toe. Similar to the camber, the toe is subjected to change as the wheel moves without any input from the steering.

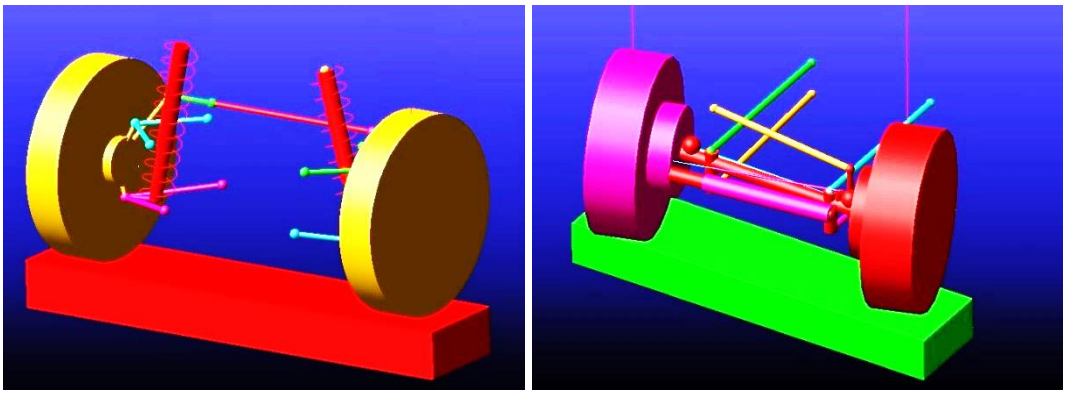

Figure 13. Gen 2.5 (left) and Gen 2(right) ADAMS Simulation setup for steering and suspension kinematics.

As described in figure 11, each axle has it's roll center about which the body rolls while experiencing any lateral acceleration. The front and the rear roll centers form the roll axis for the entire vehicle (figure 14). And as the wheels are subjected to change their position, the geometry changes too and so does the roll center location – moving the roll axis. It is important to study the roll axis migration. Although, it is debatable that the dynamic roll axis location is hard to interpret due to complex behavior of the tires and other linkage compliances [8], kinematic location is often considered a good approximation for calculation purposes.

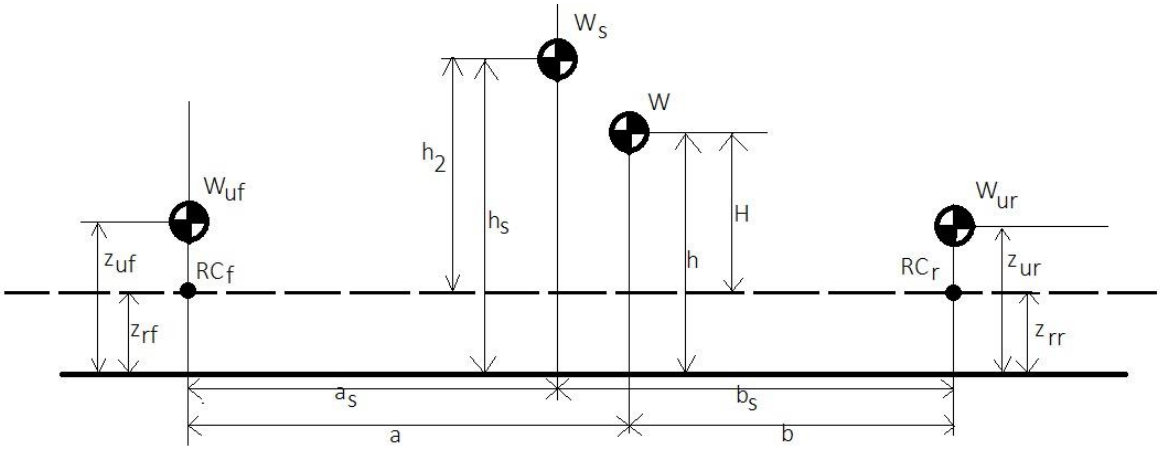

Figure 14. Roll centers RC_f and RC_r, and roll axis locations in a vehicle.

3.4 Results and Discussion

3.4.1 Wheel Alignment

The wheel alignment study was done with a sinusoidal displacement input of amplitude 2 inches to both the wheels in parallel. As discussed in section 3.2 the suspension yield roll camber of 3.9^0 on the outside wheel and the camber gain in bump has to compensate for this gain by resulting in negative camber. Figure 15 shows that the camber goes as much as -2.5^0 for the front and about -2.25^0 for the rear. Any additional compensation if required can be added by setting a static negative camber of -1.5^0. The positive camber gain in droop is less than 0.7^0 and the overall camber variation is within the desired range.

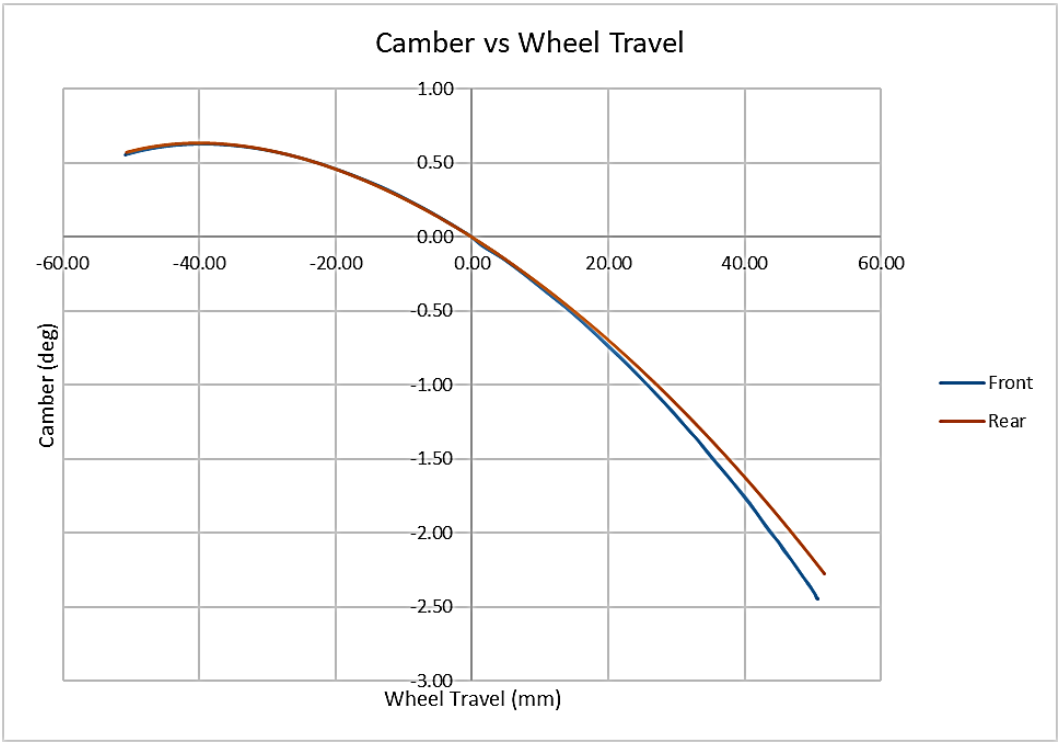

Figure 15. Camber variation against wheel travel with 0º initial camber.

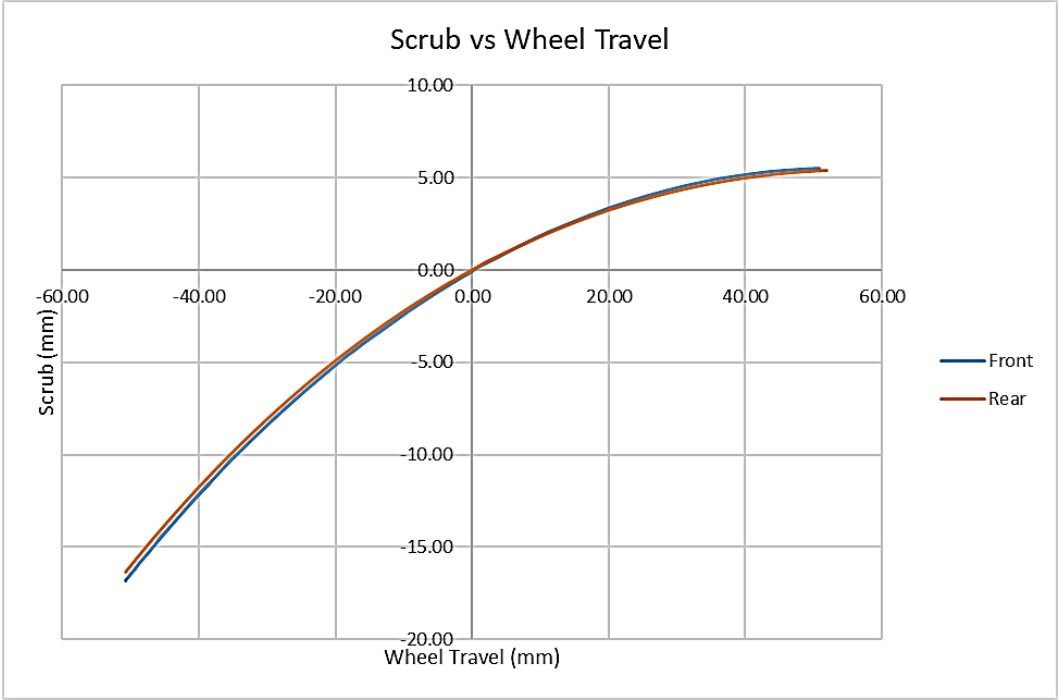

Figure 16. Lateral wheel scrub versus wheel travel.

In figure 16, it is seen that as the wheel moves up w.r.t. the frame, it moves laterally away from the frame widening the wheeltrack thus making the vehicle more stable in laden condition. The overall scrub that a wheel can experience is limited to 22 mm or less. On the same note, the laden wheel (under bump condition) only scrubs by about 5.5 mm as the rate of lateral displacement reduces as the wheel travels up w.r.t. the frame. Toe variation is another important aspect to study since it might create unbalancing forces due to ever-changing loading conditions. This phenomenon is also known as bump steer and needs to be kept as close to zero. However, small amount of toe change to inward direction can be allowed to counter the effects of any unsettling force. [9] The toe change in the front suspension (figure 17) is within 0.7^0 to -0.27^0 overall and as the wheel is laden, the toe-in increases. The toe link on the rear suspension is in-plane with the upper control arm and thus does not exhibit any toe variation.

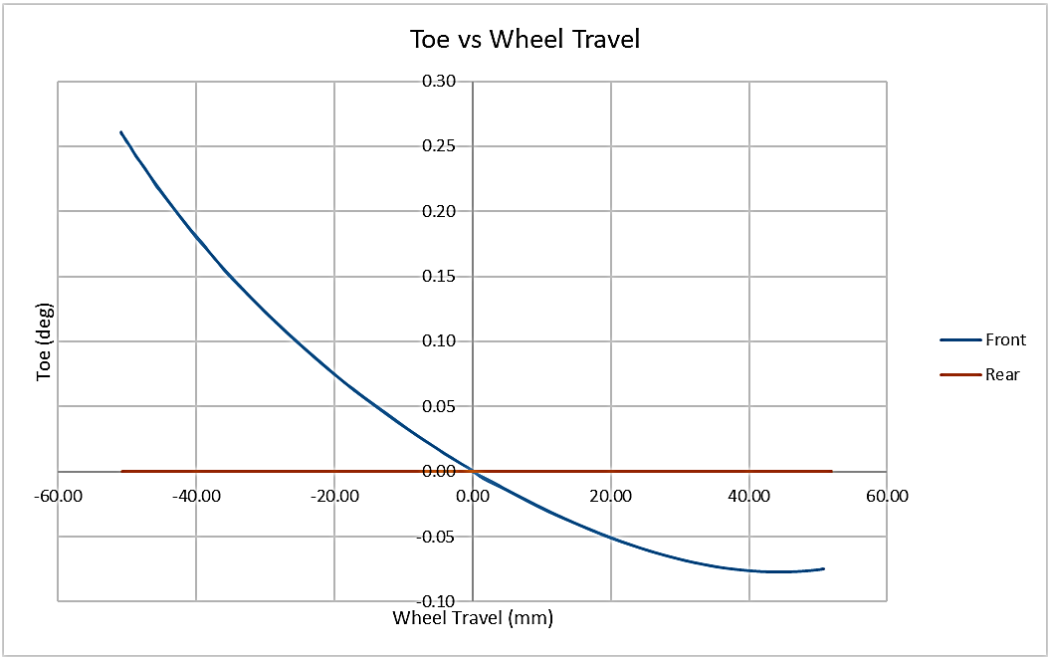

Figure 17. Toe variation versus wheel traveling front and rear suspension for Gen 2.5 vehicle.

After discussion with the team working on the vehicle's autonomous control programming, the variations in wheel alignment found above are not significant enough for current testing purposes. On-road tests will be required to establish if any modifications in current setup are needed.

3.4.2 Roll Center

Much has been written about the location and importance of roll center [5], [6], [8], [9] and its migration. Although its definition is debatable and presented in many ways, it is one of the key parameters to consider for design calculations. The roll center analysis was performed to locate the static roll center location (geometric roll center) which defines the roll center height for the front (z_{rf}) and the rear (z_{rr}) suspension. These values can be used to locate the roll axis location for dynamic modeling. Both the axles were subjected to ±2 inches (50.8 mm) bump and $\pm 8.5^0$ roll conditions to study the roll center migration. Following are the findings of the roll center analysis.

1. The static value of z_{rf} and z_{rr} are 80.9 mm and 75 mm respectively.
2. In full bump conditions, i.e. when both the wheels are fully laden to the physical limit, the roll center stays above ground. (figure 18)
3. In rolling conditions, the roll centers of both the suspensions migrate in unison towards the opposite direction of the body roll.
4. The front RC displaces between ±105 mm and the rear one between ±125 mm in lateral direction and both drop by 15 mm vertically in rolling conditions. (figures 19 and 20)
5. This amount of roll axis migration is deemed satisfactory and should result in a consistent behavior of the vehicle in dynamic conditions.

Note that any tire or suspension link compliances are not considered in this analysis.

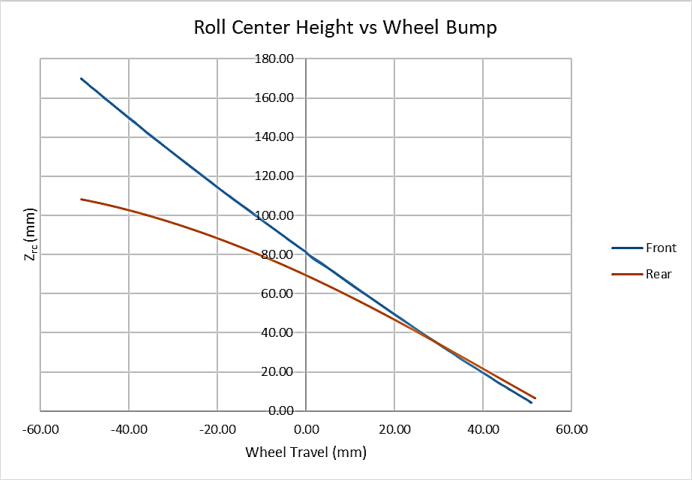

Figure 18. Roll Center height (zrc) versus wheel bump for front and rear suspension of Gen 2.5.

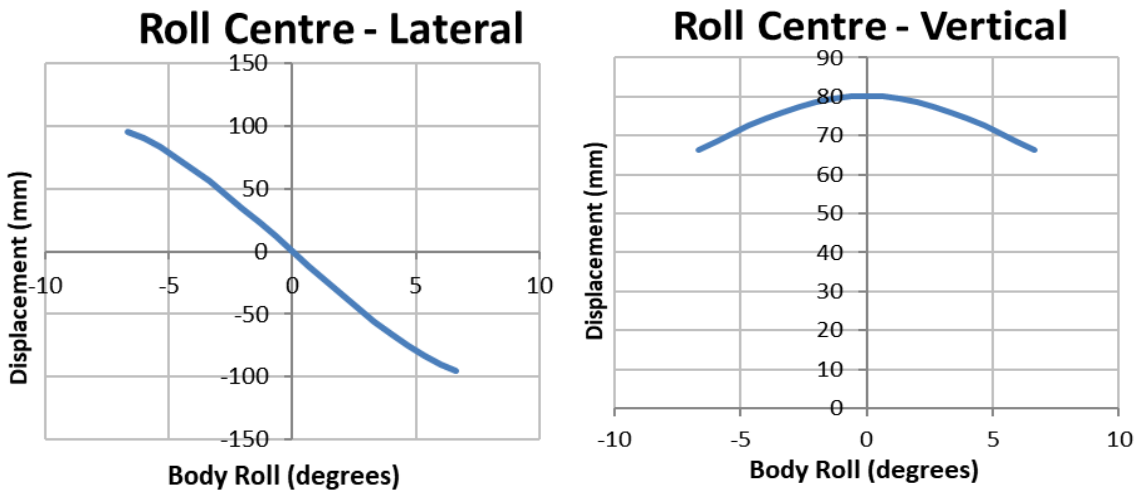

Figure 19. Lateral Roll Center migration with respect to body roll for front and rear suspension respectively.

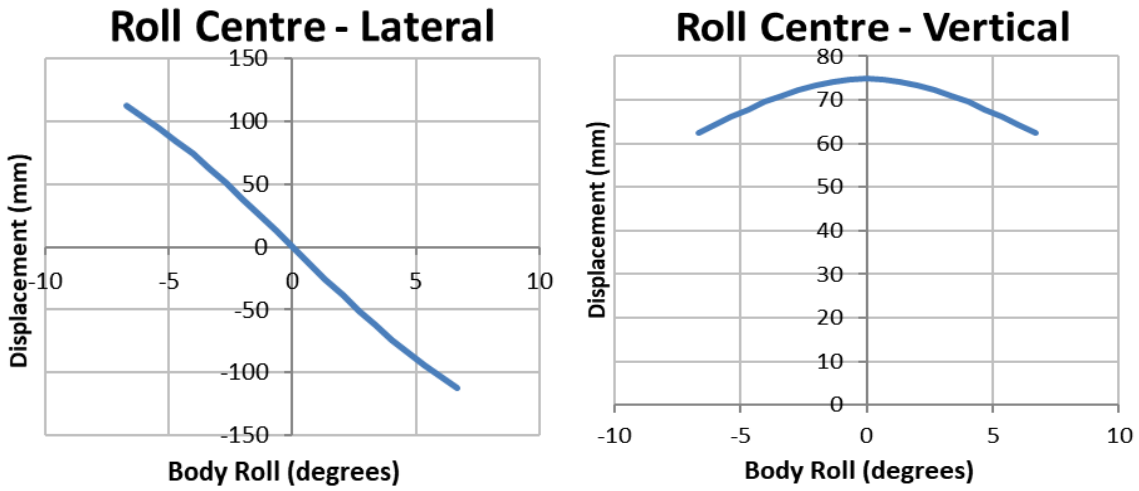

Figure 20. Vertical Roll Center migration with respect to body roll for front and rear suspension respectively.

3.4.3 Installation Ratio

The installation ratio establishes the relationship between the change in length of the spring to the wheel displacement. Usually, the suspension springs are located inside of the wheels and the wheel load to spring force ratio is determined by the installation ratio. This helps to calculate the resultant spring rate at the wheel center, thus, springs can be assumed to be located at the wheel itself while creating dynamic model of the vehicle. The installation ratio is not necessarily a constant value and may change depending upon the current wheel location. Figure 21 shows a graph of spring compression versus wheel travel and it is nearly linear, the it can be concluded that the installation ratio for this suspension can be approximated to be constant.

The installation ratios for both the axles are

$$IR_f = 0.52$$

$$IR_r = 0.49$$

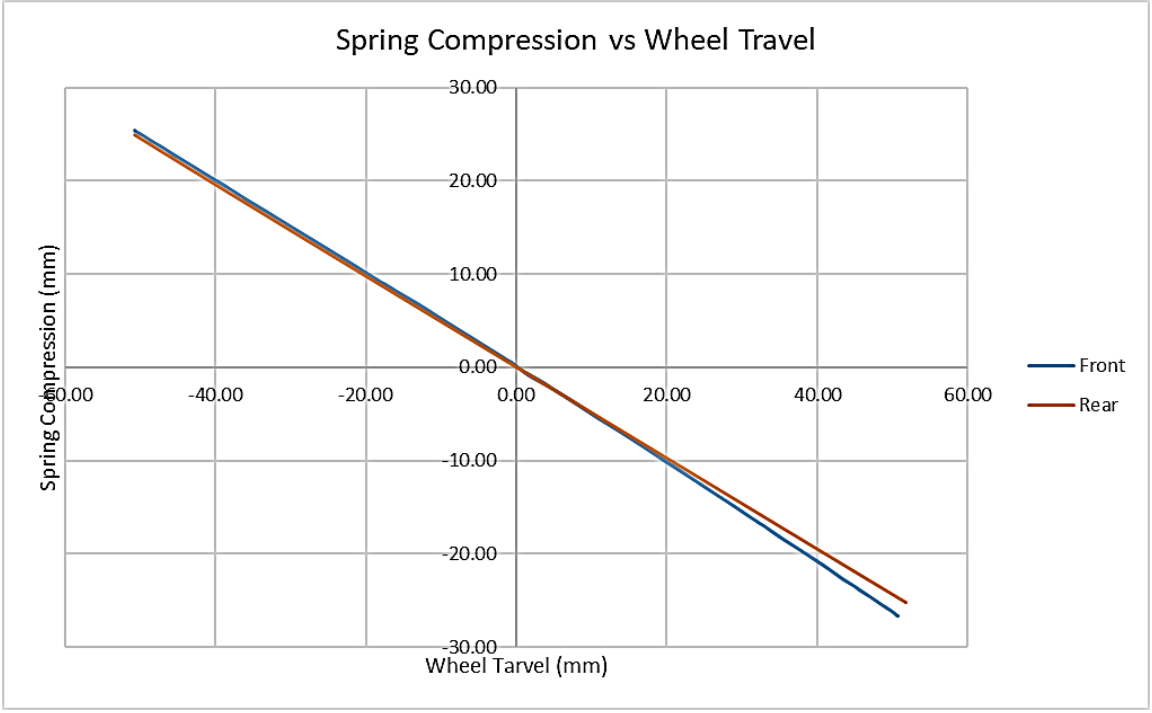

Figure 21. Spring compression versus wheel travel.

3.4.4 Steering Geometry

The gen 2 steering system was put under kinematic testing as well as Gen 2.5 to establish the relationship between the steering actuator and the toe angle of left and right wheels. Upon examination (figure 22), the steering geometry on Gen 2 displayed satisfactory behavior. As the actuator displaces from its neutral position, the toe difference between the two wheels increases steadily. However, due to physical constraints, the inner wheel cannot attain the maximum desired toe angle of 45^0.

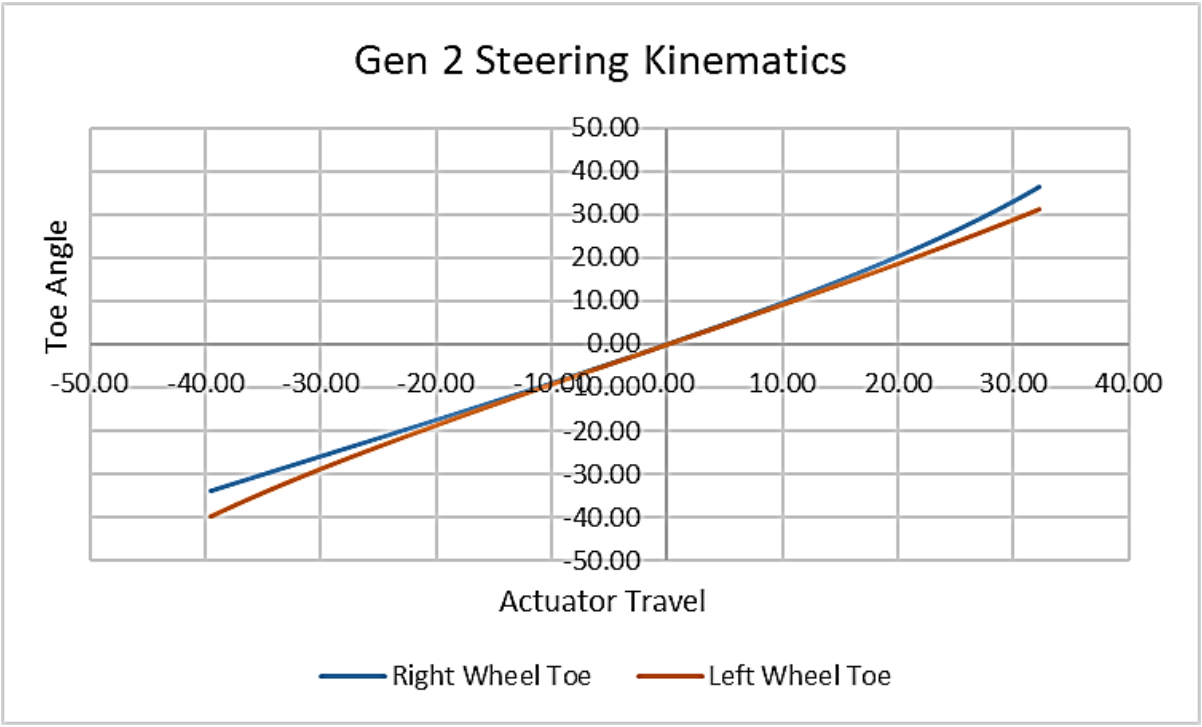

Figure 22. Front wheel steered toe angles with respect to the feedback potentiometer in Gen 2 vehicle.

Another issue with the Gen 2 steering system setup is that the actuator and the feedback sensor are not mounted parallel. Thus it was required to establish the relationship between the feedback data and the steering angle instead of the actuator. The feedback data is collected using a 12V DC linear potentiometer. The analog data from potentiometer is converted via 10bit ADC that yields current position denoted by numbers between 0 to 1023. Figure 23 shows the relationship between the two. Road tests were performed to determine the value

received from the potentiometer for ‘zero’ steering angle. Using a quadratic curve-fit an equation was generated to relate the current in potentiometer value to the current mean steering angle in radians. This relationship is given by the following equation

$$\delta_{mean} = 0.00000075P^2 + 0.0022\mathrm{P} - 1.1691 \qquad (3.4)$$

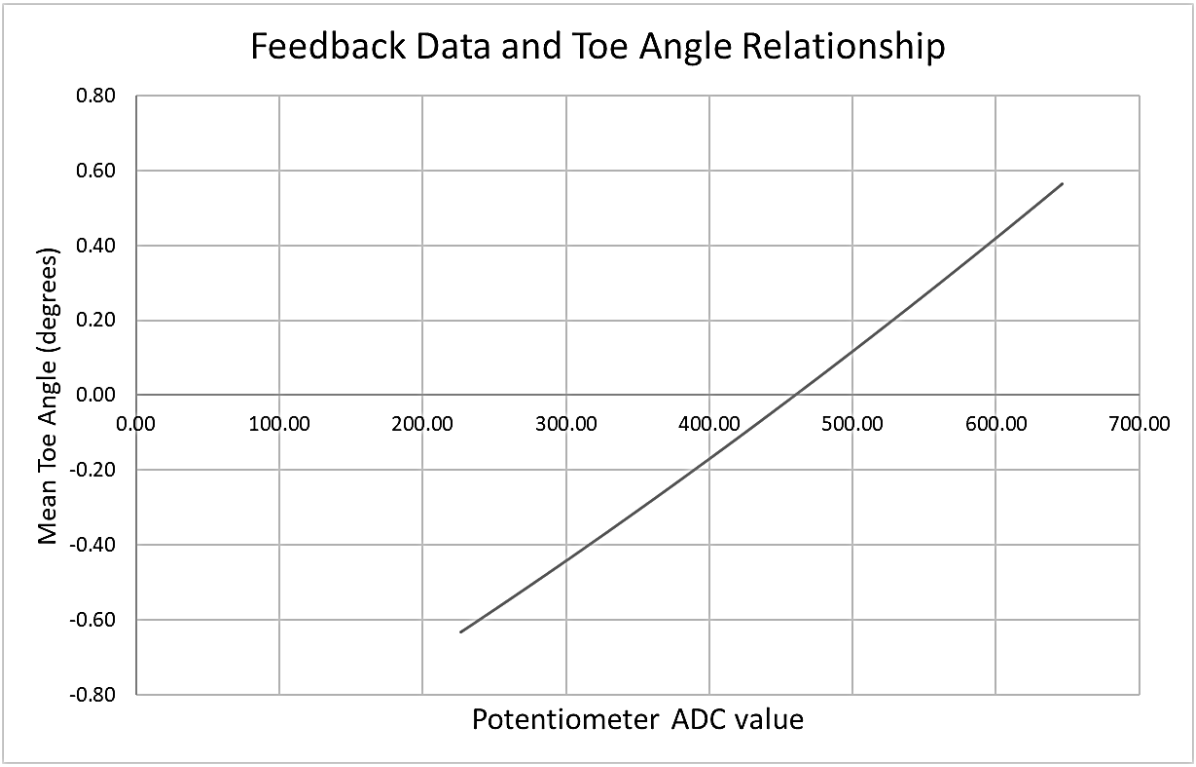

Figure 23. Feedback data from potentiometer w.r.t to the mean steering angle.

In case of the gen 2.5 steering system setup, the maximum toe angle of 45^0 for the inside wheel is achieved successfully. The steering actuator and the overall setup had to be changed to fit the space constraints, and it can be seen in figure 24 that, the toe difference between the two wheels has been reduced when compared to the gen 2 setup. One way to describe the kinematic relationship between the left and right wheel steering toe is by calculating the Ackermann Percentage. Ackerman percentage indicates the error in the toe angles difference between the current and ideal values. The ideal geometry may depend upon the type and purpose of the vehicle, which will determine the inside or the outside wheel to be

the ‘ideal one’ and the error in the toe angle is compared to what it should be according to the perfect Ackermann geometry. A third way of measuring the error is by considering the mean turning radius. [10] The method is given below (figure 24).

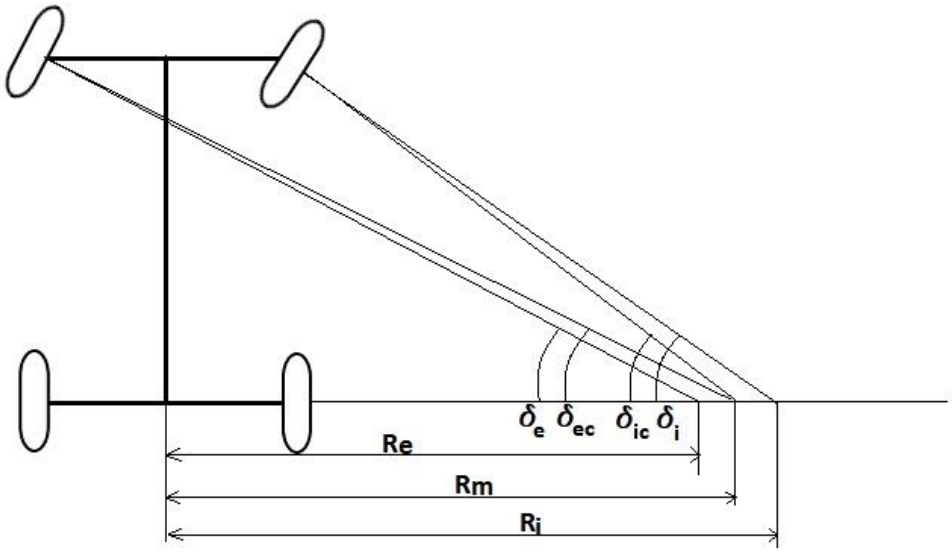

Figure 24. Ackermann percentage calculation method by mean turning radius method.

Consider the plane view as shown in the above diagram. The left wheel is turned by an angle δ_e and the right wheel is turned by an angle δ_i. According to the perfect Ackermann geometry, the point about which all the wheels should lie on the line extended horizontally along the rear axle to cause perfect rolling of the wheels without slipping. Since, this configuration is not achieved at every cornering instant, the error in the geometry is measured by the following method. Considering that some error exists, with the current angles δ_e and δ_i, assume that the point where the turning axis of external wheel intersects the extended rear axle to be at a distance of R_e, i.e. the turning radius of the outer wheel. Similarly, there is R_i associated with the inner wheel. The mean of these radii is calculated to be R_m. The angles required to be made by the outer and the inner wheel to have their turning axes intersect at R_m are calculated to be δ_{ic} and δ_{ec} respectively.

Then the percentage of Ackermann is given by

$$\%Ackermann = \frac{\delta_i - \delta_e}{\delta_{ic} - \delta_{ec}} \; x \; 100 \qquad (3.5)$$

Both steering setups are 50% pro-Ackermann at the neutral (zero steering angle) position, but the percentage declines for the Gen 2.5 whereas it increases for the Gen 2 steering setup. No comments can be made yet as in which setup behaves better, but steady state cornering tests can be performed with both the generations and compare their behavior under similar conditions.

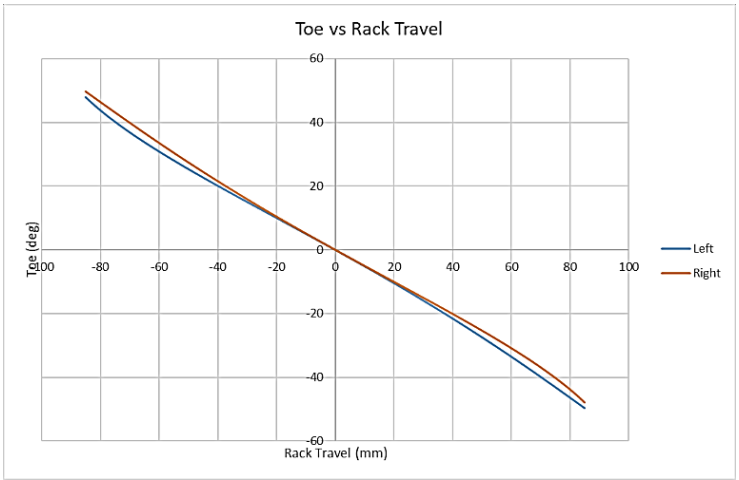

Figure 25. Front wheel steered toe angles with respect to the linear actuator in Gen 2.5 vehicle

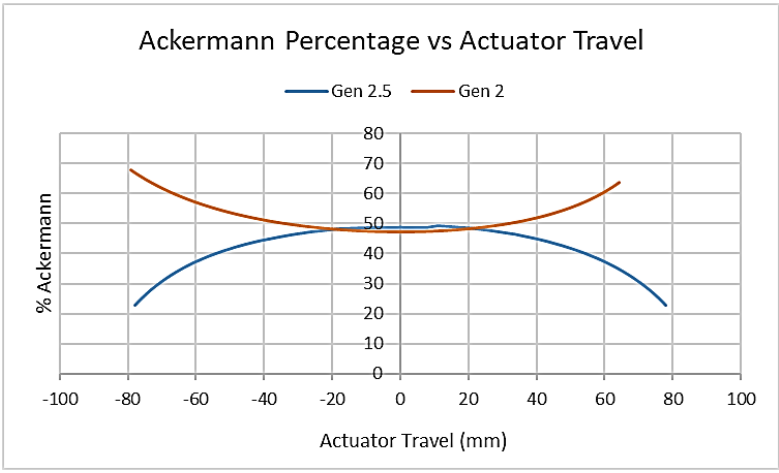

Figure 26. Ackermann percentage comparison for Gen 2 and Gen 2.5 Steering setup.

Another kinematic aspect to consider was the effect on the toe angle due to wheel travel. The steering actuator is mounted on the frame and the tie rod connects the wheel and the actuator with swivel joints. Thus the rack, the frame and the wheel change their position with each other at the same time. The steering system was actuated at maximum droop (-50.8 mm), neutral and maximum bump (50.8 mm) and the actuator and toe angle relationship was plotted (figure27). It is seen that as the actuator moves away from the center, the change in toe can be significant – about 5^0. The steering toe angle behavior is fit with a linear curve with 'x' as the rack displacement is given as

$$\delta_{mean} = -0.5456x \qquad (3.5)$$

And the change in this curve is nothing but change in the slope value depending upon the wheel's vertical displacement as given in table 4.

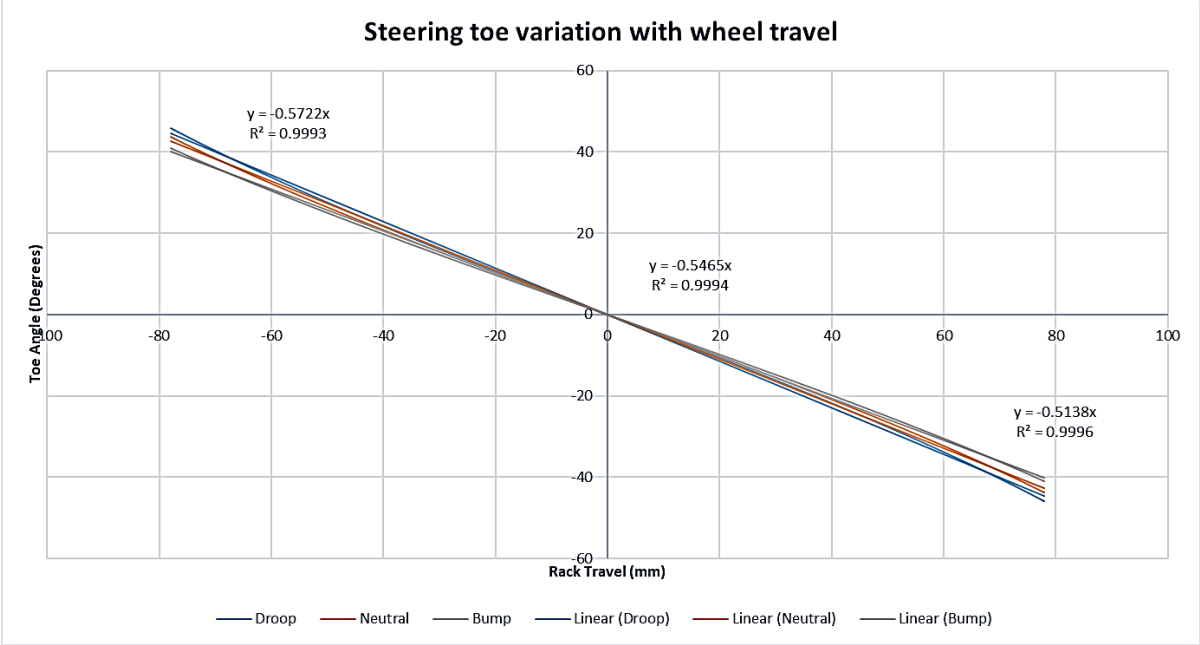

Figure 27. Steering angle – actuator travel relationship with different wheel positions.

Table 4. Steering angle equation variation with different wheel positions.

Wheel Displacement	Slope	Δ slope
-50.8 mm (droop)	-0.5138	-0.318
0 mm	-0.5456	0
50.8 mm (Bump)	-0.5722	+0.266

3.4.5 Roll Effects on Steering

The effects of the body roll on the wheel alignment in terms of camber and toe induce steering effects. The change in the alignments are shown in figure 28. It is seen that the due to the large amount of body roll, a similar degree of roll camber in induced in the wheels, however, the bump camber gain reduces the roll camber gain of the laden wheel. The mean gradient for the roll camber and roll steer is taken for the front axle.

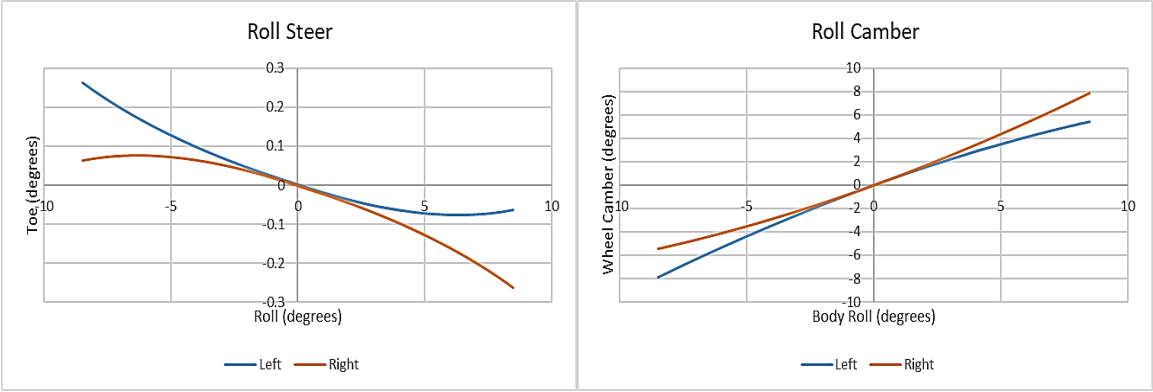

Figure 28. Roll effects on camber and toe

Roll Camber Gradient = 0.775 deg/deg roll

Roll Steer Gradient = - 0.02 deg/deg roll

CHAPTER 4: ROLLOVER MODEL AND RIDE ANALYSIS

Rollover is one of the most important safety aspects of an automobile. Rollover can be defined as the rotation of the vehicle of 90^0 or more about its longitudinal axis. EcoPRT prototype vehicles have a high center of gravity given their narrow wheel track. Thus, their susceptibility to rollover conditions is an important factor to consider. This chapter conducts a study to determine static rollover thresholds and establish other parameters like spring stiffness, anti-roll bar stiffness and their influence on dynamic rollover model.

4.1 Steady State Rollover Model

NHTSA has identified three metrics to parameterize a vehicle's vulnerability to roll over. [11], [12] These metrics consider the vehicle to be rigid body as shown in figure 29. A general model of a rigid body vehicle is considered to be standing on a banked road. The tire and suspension deflections are not considered. As the vehicle undergoes a turn, a centripetal force acts on the vehicle generated by tires turning it into the corner, and at the same time, centrifugal force acts on the body in the opposite direction.

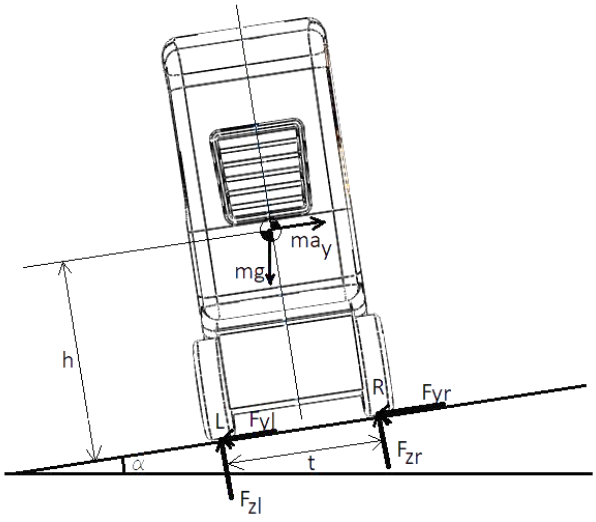

Figure 29. Rigid vehicle model.

Consider the mass of the vehicle to be ‘m’, the CG to be located at a height ‘h’ and the track width to be ‘t’. F_{zr} and F_{zl} are the normal forces at the right and the left wheel respectively, and F_{yr} and F_{yl} are the lateral forces. a_y is the centripetal acceleration of the vehicle. Taking the moment at the right wheel ‘R’, the Newton's second law equation can be written as,

$$I_{xR}\ddot{\phi} = F_{zl}t - (mg\ sin[\alpha])h - (mg\ cos[\alpha])\frac{t}{2} + ma_y h \qquad (4.1)$$

Usually, the banking angle is very small and since the assumed condition is steady state, the rotational acceleration is neglected.

$$\sin[\alpha] = \alpha, \qquad \cos[\alpha] = 1, \quad \text{and} \quad \ddot{\phi} = 0$$

Therefore, equation 4.1 can be rewritten as

$$F_{zl}t - mgh\alpha - mg\frac{t}{2} + ma_y h = 0 \qquad (4.2)$$

The above equation will be used to calculate the three rollover stability metrics in the following sections.

4.1.1 Static Stability Factor

The static stability factor (SSF) is the most basic of the rollover safety standards. As per the model described above, the rollover is considered to begin when the normal load on the left wheel is zero. Thus, ht e equation 4.2 can be written as

$$mgh\alpha - mg\frac{t}{2} + ma_y h = 0$$

Which reduces to,

$$\frac{a_y}{g} = \frac{t}{2h} + \alpha \qquad (4.3)$$

If the road has no banking angle, i.e. α = 0, then what we get is the static stability factor.

$$\boldsymbol{\frac{a_y}{g} = \frac{t}{2h}} \qquad (4.5)$$

4.1.2 Tilt Table Ratio

The Tilt Table Ratio (TTR) test considers the vehicle to be placed on an inclined table that can be tilted from the horizontal by an angle α. Unlike the SSF test, TTR considers the resolved force parallel to the table due to vehicle's weight as the centripetal force. The table is gradually tilted until the wheels on the upper side of the platform lose the contact. This moment, the ratio of the lateral to the vertical weight component equals the tangent of the tilt angle 'α.'

$$TTR = \ tan[\alpha] = \frac{mg\ sin[\alpha]}{mg\ cos[\alpha]} \tag{4.6}$$

For most light-duty vehicles, the tilt angle at which the rollover occurs, the TTR is expected to be 60 to 80%. [7], [11]

4.1.3 Side Pull Ratio

The Side Pull Ratio (SPR) provides better estimate of rollover threshold for vehicles with inherently better stability (wide track or low CG) than SSF and TTR. In this test, the vehicle is placed on a horizontal table and is pulled to its side with a cable at the height of its CG. A curb is placed at the wheels to resist the pull of the cable. The SPR is defined by the ratio of the pull force required to lift one side of the vehicle to the weight of the vehicle.

$$SPR = \frac{F_{pull}}{mg} \tag{4.5}$$

4.1.4 Results

All the tests described in the above sections are not to be confused as the absolute thresholds for the rollover conditions but they are simplified means to analyze or compare rollover stability of vehicles. The gen 2 and 2.5 vehicles are compared against each other using above standards and the results are as follows.

Table 5. Rollover stability comparison of gen 2 and 2.5 vehicle.

Test	Gen 2	Gen 2.5
SSF	0.543g	0.622g
TTR	0.536	0.614
SPR	1.543	1.622

4.2 Suspended Vehicle Model

Now that it is established that the gen 2.5 model is more stable than its predecessor, a more accurate representation of rollover stability can be realized by considering suspension and tire deflections. This section will study the suspended vehicle model (figure 30) to establish requirements for the suspension spring stiffness. For simplicity, the model assumes two different mass bodies of sprung and unsprung mass instead of three (left and right wheel are independent masses in SLA suspension). Note that the purpose of this study is only to find the minimum required parameters and not to finalize them.

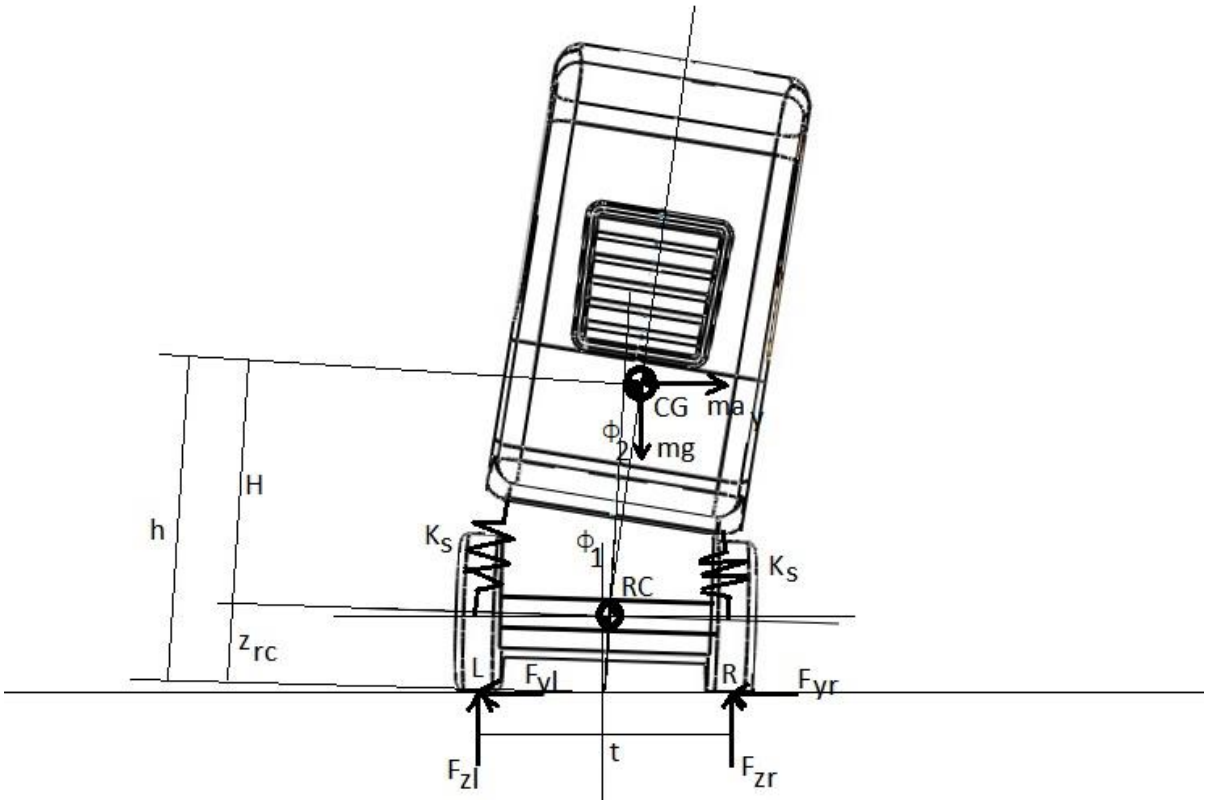

Figure 30. Suspended Vehicle Model.

The vehicle model is considered to undergo steady state cornering condition towards left-hand side. Because of the tires and suspension, the right-hand side will be compressed and the CG will shift towards right, reducing the rollover threshold. In the above figure, the suspension rolls about the longitudinal axis by an angle Φ_1 and the body rolls about the roll

axis w.r.t the suspension by an angle Φ_2. The roll axis is assumed to be passing longitudinally through the roll center RC. The total body roll occurring at rollover is $\Phi_1 + \Phi_2$. Applying the second law of Newton and considering the moment at the right wheel 'R'

$$F_{zl}t + ma_y(z_{rc}\,cos[\phi_1] + Hcos[\phi_1 + \phi_2]) \ldots$$

$$\ldots - mg\left(\frac{t}{2} - z_{rc}\,sin[\phi_1] - Hsin[\phi_1 + \phi_2]\right) = I_{xR}\ddot{\phi} \qquad (4.6)$$

For steady state conditions, $\ddot{\phi} = 0$, and ϕ_1 and ϕ_2 are small, also, at the beginning of the rollover, F_{zl} is zero. Thus,

$\cos\phi_1 = 1$, $\cos(\phi_1 + \phi_2) = 1$, $\sin\phi_1 = \phi_1$, and $\sin(\phi_1 + \phi_2) = (\phi_1 + \phi_2)$

The equation 4.6 can be rewritten as

$$ma_y(z_{rc} + H) - mg\left(\frac{t}{2} - z_{rc}\phi_1 - H(\phi_1 + \phi_2)\right) = 0$$

$$\frac{a_y}{g} = \frac{t}{2h} - \phi_1 - \frac{H}{h}\phi_2 \qquad (4.7)$$

Comparison between equations 4.5 and 4.7 shows that the suspended vehicle model includes the deflections due to both the tires and the suspension and are both negative terms reducing the rollover threshold. The following sections deal with the calculation of tire and suspension deflection.

4.2.1 Tire Deflection

In this section, only the tires are considered to be deflected ignoring the suspension. Considering the rollover situation, the entire mass is supported by the outside wheels. For a

symmetric vehicle, half of its mass is supported by either side, thus the total change in the load on the outside tires is

$$\Delta F = \frac{mg}{2} \tag{4.8}$$

Consider K_t to be the stiffness of the tires and Δr to be the outside tire deflection, then

$$\Delta r = \frac{\Delta F}{K_t} = \frac{mg}{2K_t} \tag{4.9}$$

The deflection angle of the axle can be given by

$$\phi_1 = \frac{\Delta r}{t/2} = \frac{mg}{tK_t} \tag{4.10}$$

4.2.2 Suspension Deflection

Now that the tire deflection is known, the suspension deflection can be calculated. For simplicity, the springs are considered mounted directly on top of the tires (figure 28), i.e. the spring rate considered here is the wheel rate. Let Δs be the compression of the spring on the outer side. Then the body roll w.r.t. the axle is

$$tan\phi_2 = \frac{\Delta s}{t/2} \tag{4.11}$$

ϕ_2 is small, thus $tan\phi_2 = \phi_2$

The equation 4.11 can be rewritten as

$$\Delta s = \frac{t\phi_2}{2} \tag{4.12}$$

This model considers that the wheel forces are transferred through the springs. It is also assumed that the body rolls w.r.t the axle about its roll center 'RC.' Taking the moment about the RC, we obtain

$$ma_y H cos[\phi_1 + \phi_2] + mgHsin[\phi_1 + \phi_2] - F_s t = I_{xRC}\ddot{\phi} \tag{4.13}$$

The term F_s in above equation is the spring force, and the term F_s indicates the roll stiffness. The spring force, from equations 4.11 and 4.12 is given by

$$F_s = K_s \Delta s = K_s \frac{t\phi_2}{2} \tag{4.14}$$

Where K_s is the spring stiffness. Also, for steady-state cornering, $\ddot{\phi} = 0$, and ϕ_1 and ϕ_2 are considered small. The equation 4.13 is rewritten as

$$ma_y H + mgH[\phi_1 + \phi_2] - \frac{t^2}{2} K_s \phi_2 = 0$$

i.e. $$\phi_2 = \frac{a_y}{g} \frac{mgH}{\frac{t^2}{2} K_s - mgH} + \frac{mgH}{\frac{t^2}{2} K_s - mgH} \phi_1 \qquad (4.15)$$

4.3.3 Suspension Spring Stiffness

The calculations for suspension and tire deflections can be now made and more accurate predictions about rollover threshold can be delivered. The following can be concluded from equations 4.7, 4.10 and 4.15.

1. The track width is directly proportional to the rollover threshold. Wider wheel track will yield higher stability factor.
2. The rollover angle is heavily influenced by the suspension stiffness K_s. Larger the stiffness, smaller the body roll.
3. The distance between the RC and the CG is also important factor in creating the roll moment arm.
4. Looking at equation 4.15, for a stable behavior, the value of ϕ_2 should be positive. i.e.

$$\frac{t^2}{2} K_s - mgH \geq 0 \qquad (4.16)$$

Thus, $K_s \geq \frac{2mgH}{t^2}$ i.e $K_s \geq 10{,}528.63\ N/m$

The objective of this study is to determine the minimum spring stiffness required so that the rollover threshold obtained after considering the tire and suspension deflections is still close to the SSF found in section 4.1. From equations 4.7, 4.10 and 4.15

$$\frac{a_y}{g} = \left(\frac{t}{2h}\right) - \left(\frac{mg}{tK_t}\right) - \left(\frac{H}{h}\frac{a_y}{g}\right)\frac{mgH^2}{\frac{t^2}{2}K_s - mgH} + \frac{mgH^2}{\frac{t^2}{2}K_s - mgH}\left(\frac{mg}{tK_t}\right) \quad (4.17)$$

In the above equation, the term $\frac{t^2}{2}K_s$ represents roll stiffness provided by the springs which can be replaced by $K_{\Phi s}$. Also, it is seen that the body roll is also a function of lateral acceleration a_y.

Thus, after simplifying we get,

$$\frac{a_y}{g} = \left(\frac{t}{2h}\right) - \left(\frac{t}{2h}\right)\left(\frac{mgH^2}{hK_{\Phi s} - mghH + mgH^2}\right) - \left(\frac{mg}{tK_t}\right) \quad (4.18)$$

The second and third terms in the above equation are the compliances due to the suspension and tire deflection. The tire deflection is constant but the suspension deflection will depend upon the choice of roll stiffness. To get an idea of the minimum roll stiffness required, the rollover threshold was plotted for a range of roll stiffness values as shown in figure 31.

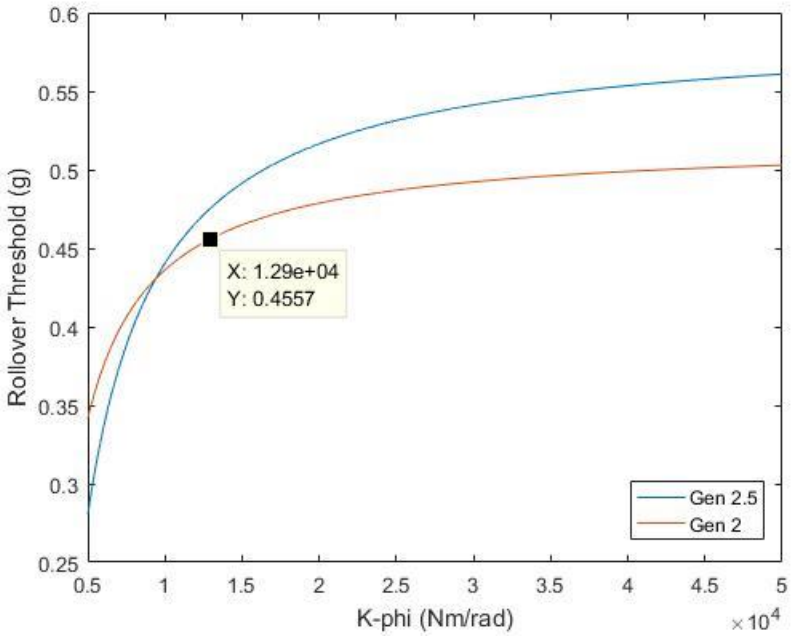

Figure 31. Rollover threshold versus roll stiffness due to suspension springs

It is seen that the roll stiffness has great impact on the rollover threshold. Although, the threshold increases with the roll stiffness, it asymptotes to a certain value below the SSF. The choice of roll stiffness will also impact the ride stiffness and frequencies, thus choosing the right value is important. Looking at the graph (figure 29), a value above 15,000 Nm/rad should be safe enough.

4.3 Ride and Roll Rates

As the minimum requirements for the vehicle's roll stiffness are known. Some reasonable approximations could be made for spring rates calculations for the gen 2.5 suspension setups. The following procedure is analogous to the one described in Milliken. [6] This method starts with an assumed cornering conditions and a few parameters and the verifying the results with the desired performance.

The basic car can be described by the following information gathered from the CAD model.

$W_f = 2750$ N	$W_1 = 1375$ N	$W_2 = 1375$ N	(Front load)
$W_r = 2250$ N	$W_3 = 1125$ N	$W_4 = 1125$ N	(Rear load)
$W_t = 5000$ N			(Total load)
$t_f = t_r = 0.711$ m			(Track width)
$l = 1.778$ m			(Wheelbase, CG location)
$h = 0.62$ m			(CG height)
$H = 0.542$ m			(Roll axis to CG distance)

4.3.1 Simulated Cornering Condition

Assume a left hand (+ve) cornering condition with following values (figure 30)

$\alpha = 10$ deg	(Angle of banking)
$R = 50$ m	(Turn radius)
$V = 34$ mph ≈ 15 m/sec	(travel speed)

According to suspension geometry designed for gen 2.5

z_{rf} = 0.0809 m z_{rr} = 0.075 m (Roll center heights)

z_r = 0.0779 m (Roll Axis height)

Also, assuming no drive torque and longitudinal acceleration. Now, for the first pass of the calculations, assuming following roll rates for getting the target roll gradient.

$K_{\varphi f}$ = 8000 Nm/rad $K_{\varphi r}$ = 7000 Nm/rad ($K_{\varphi f}$ + $K_{\varphi r}$ = 15000Nm/rad)

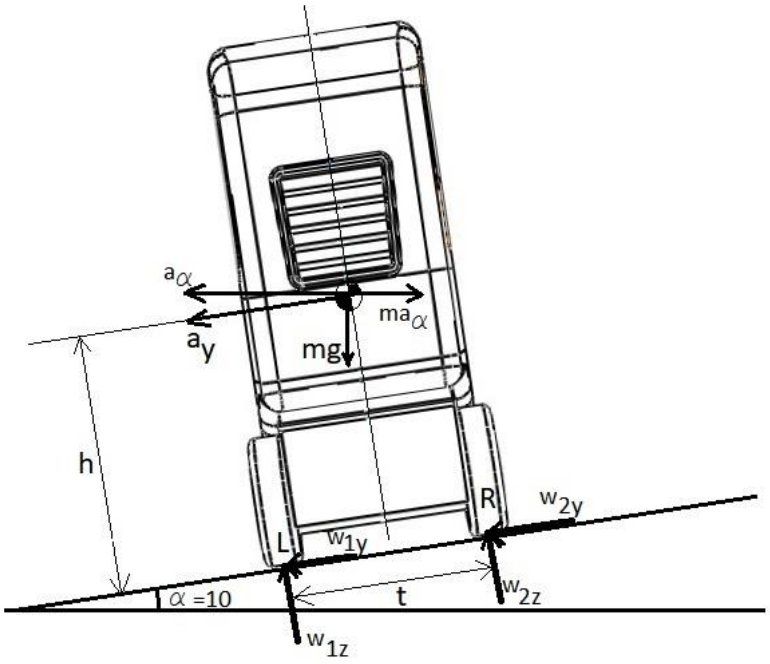

Figure 32. Steady state cornering on a banked road

The lateral acceleration is given by

$$A_\alpha = \frac{V^2}{g\,R} = \frac{15^2}{9.81\,x\,45} = 0.5091\text{g} \qquad (4.19)$$

Taking summation of lateral and vertical forces,

$$\Sigma F_y = -ma_\alpha \cos\alpha + mg \sin\alpha = ma_y \quad (4.20)$$

$$\Sigma F_z = -ma_\alpha \sin\alpha - mg \cos\alpha = -W' \quad (4.21)$$

The summation of vertical force is analogous to the total load acting on the road and the equation 4.20 can be rewritten to find the lateral acceleration in vehicle's frame of reference.

$$a_y = -a_\alpha \cos\alpha + g \sin\alpha \qquad \text{OR dividing both sides by g}$$

$$A_y = -A_\alpha \cos\alpha + \sin\alpha = -0.3284 \text{ g} \quad (4.22)$$

Effective total weight due to the banking and the individual weights on each axle are

$$W' = ma_\alpha \sin\alpha + mg \cos\alpha = 5366 \text{ N} \quad (4.23)$$

$$W'_f = W' \frac{b}{l} = 2951.5 \text{ N} \quad (4.24)$$

$$W'_r = W' \frac{a}{l} = 2414.9 \text{ N} \quad (4.25)$$

The body roll angle is given by

$$\phi = \frac{Force\ x\ Moment\ Arm}{Total\ Roll\ Stiffness} = \frac{(W' A_y)\ H}{K_{\phi f} + K_{\phi r}} \quad (4.26)$$

Therefore, the roll gradient is

$$\frac{\phi}{A_y} = \frac{W' H}{K_{\phi f} + K_{\phi r}} = -0.1808 \text{ rad/g} = -10.359 \text{ deg/g} \quad (4.27)$$

The table 6 given below shows the typical values for the roll gradients depending upon the type of a vehicle. As the assumed roll stiffness is not enough to match the typical values, a

few iterations were performed to get the roll gradient within the range of typical family sedans with soft and comfortable suspension.

Table 6. Typical Roll Gradients for different types of vehicles.[6]

Vehicle Genre	**Roll Gradient (deg/g)**
Very soft to soft – Domestic and import family cars	8.5 – 7.5
Semi-soft – Contemporary mid-market sedans	7.0
Semi-firm – Imported sport sedans	6.0
Firm – Domestic sport sedans	5.0
Very firm – High-performance domestic cars	4.2
Extremely Firm – Sports cars/ Hyper-cars	3.0
Hard – Racing Cars only	1.5

The final roll rates chosen for the front and rear suspension are

$K_{\varphi f}$ = 10170 Nm/rad $K_{\varphi r}$ = 9145 Nm/rad $K_{\varphi f} + K_{\varphi r}$ = 19315 Nm/rad) (4.28a)

And the new roll gradient is

$$\frac{\phi}{A_y} = \text{- 8.04 deg/g.} \quad (4.28b)$$

The rollover threshold at this stiffness is 0.5138g.

Now, to find the lateral load transfer on each axle, the car is assumed to be distributed in three bodies. Two unsprung bodies as axles and the sprung mass. (Refer to figure 14). The front and rear load transfers due to lateral acceleration are given as:

$$\Delta W_f = A_y \frac{W}{t}\left(\frac{K_{\Phi f}\ H}{K_{\Phi f}+K_{\Phi r}} + \frac{b}{l}\ z_r\right) = \text{- 699.11 N} \quad (4.29)$$

$$\Delta W_r = A_y \frac{W}{t}\left(\frac{K_{\Phi r}\ H}{K_{\Phi f}+K_{\Phi r}} + \frac{a}{l}\ z_r\right) = \text{- 621.26 N} \quad (4.30)$$

*Refer Appendix A3 for detailed derivation of equations 4.29 and 4.30.

4.3.2 The Individual Wheel Loads

As the load transfer on each axle is known, the instantaneous loads on individual wheels can be calculated. The outside wheels gain the load while the inside wheels lose it by the same amount.

Front Outside: $W_{fo} = 2951.5/2 + 699.11 = 2174.86$ N (4.31a)

Front Inside: $W_{fi} = 2951.5/2 – 699.11 = 776.64$ N (4.31b)

Rear Outside: $W_{ro} = 2414.9/2 + 621.26 = 1828.71$ N (4.31c)

Rear Inside: $W_{fi} = 2414.9/2 – 621.26 = 586.19$ N (4.31d)

And the total effective change in the wheel loads from the static level position of the vehicle to the current cornering condition is:

Front Outside: $\Delta W_{fo} = 2174.86 – 1375 = +799.86$ N (4.32a)

Front Inside: $\Delta W_{fi} = 776.64 – 1375 = -598.36$ N (4.32b)

Rear Outside: $\Delta W_{ro} = 1828.71 – 1125 = +703.71$ N (4.32c)

Rear Inside: $\Delta W_{fi} = 586.19 – 1125 = -538.81$ N (4.32d)

According to the above values, it is possible to assume suitable wheel rates. Considering the available jounce travel of 2 inches, a portion of the travel height (40 mm out of 50.8 mm) can be yielded for this scenario, leaving the remaining distance for braking, acceleration or localized bumps on the road.

$$K_{rf} = 799.86/0.04 = 19996.5 \text{ N/m} \quad (4.33a)$$

$$K_{rr} = 703.71/0.04 = 17.592.75 \text{ N/m} \quad (4.33b)$$

4.3.3 The Ride Frequencies

The ride frequencies can now be calculated. Considering the quarter car model, the corner weight on the front is half the W_f.

$$\omega_f = \frac{1}{2\prod}\sqrt{\frac{K_{rf}\, g}{w_f/2}} = 1.902 \text{ Hz} = 114.12 \text{ cpm} \quad (4.34)$$

To minimize the body pitch on bumps while traveling in the forward direction, the rear frequency should be about 15% more than that of the front. [13]

Assume that $\omega_r = 2.187 \text{ Hz} = 131.22 \text{ cpm}$ (4.35)

Thus, the updated rear ride rate is

$$\omega_r = \frac{1}{2\prod}\sqrt{\frac{K_{rr} g}{w_r/2}}$$

$$K_{rr} = 23122 \text{ N/m} \quad (4.36)$$

The suspension frequencies calculated for this vehicle are still high when compared to a typical passenger car. These values are a result of choosing a short ride travel.

Now, to calculate the contribution of suspension springs to the roll rates.

$$K_{\varphi f} = \frac{K_{rf}\, t_f^2}{2} = 5943.5 \text{ Nm/rad} \quad (4.37)$$

$$K_{\varphi r} = \frac{K_{rr}\, t_r^2}{2} = 6872.5 \text{ Nm/rad} \quad (4.38)$$

Since the above roll rates are only due to the springs, additional roll stiffness needs to be added by means of anti-roll bars. The anti-roll bars are twist beams that connect the two wheels on the same axle. They do not affect the ride rate but only work in case of opposite wheel travel/rolling condition. This secondary connection makes the suspension indirectly

dependent, but as long as the total roll stiffness added to the suspension due to roll bars is less than 50%, it does not have a large impact on the independent behavior of the wheels. [14]

Assuming the spring rate of a radial ply tire at 35psi air pressure to be 200000 N/m. Then, the wheel center rates can be calculated considering springs-in-series setup.

$$K_{wf} = \frac{K_{rf}\, K_t}{K_t - K_{rf}} = 22218 \text{ N/m} \quad (4.39)$$

$$K_{wr} = \frac{K_{rr}\, K_t}{K_t - K_{rr}} = 26145 \text{ N/m} \quad (4.40)$$

Since the wheel center rate is known, it is now possible to find the additional roll stiffness that needs to be provided by the anti-roll bar. Consider that $K_{\Phi fdes}$ and $K_{\Phi r\,des}$ are the desired roll rates as found in equations 4.28. Applying the springs-in-series law, we get

$$K_{\varphi Bf} \frac{K_{\Phi fdes}\left(K_t\, t^2/_2\right)}{\left(K_t\, t^2/_2 - K_{\Phi fdes}\right)} - K_{wf}\, t^2/_2 = 5665.3 \text{ Nm/rad} \quad (4.41)$$

$$K_{\varphi Br} = \frac{K_{\Phi rdes}\left(K_t\, t^2/_2\right)}{\left(K_t\, t^2/_2 - K_{\Phi rdes}\right)} - K_{wr}\, t^2/_2 = 3036.8 \text{ Nm/rad} \quad (4.42)$$

4.3.4 Spring Rates

Considering the Installation ratio at the neutral position of the wheel as found in section 3.4.3, the spring rates can be calculated as,

$$K_{sf} = \left(\frac{K_{wf}}{IR^2}\right) = \frac{22218}{0.52^2} = 82171 \text{ N/m} \quad (4.43)$$

$$K_{sr} = \left(\frac{K_{wr}}{IR^2}\right) = \frac{26145}{0.49^2} = 108892 \text{ N/m} \quad (4.44)$$

4.3.5 Anti Roll Bar Rates

According to the available space, following values for the ARB are considered.

L = 0.095 m (ARB lever arm length)

I_B = Installation ratio = 0.23

Let $K_{\varphi B}$ be the ARB stiffness at the mounting and $K_{\theta B}$ the twist beam stiffness. Thus,

$$K_{\theta Bf} = K_{\varphi Bf} \frac{L^2}{t^2 \, x \, I_B^2} = 1625.79 \text{ Nm/rad} = 28.4 \text{ Nm/deg} \quad (4.45)$$

$$K_{\theta Br} = K_{\varphi Br} \frac{L^2}{t^2 \, x \, I_B^2} = 871.48 \text{ Nm/rad} = 15.2 \text{ Nm/deg} \quad (4.46)$$

4.4 Ride Analysis

Vehicle's travel on a variety of surfaces and receive vibrational inputs continuously while moving. The suspension spring-damper system tends to isolate the frame or the passengers from these road vibrations. Often, the 'quality' of any vehicle is judged by the isolation behavior of the vehicle's suspension. This dynamic behavior can be characterized by studying input versus output behavior. For simplicity, the vehicle can be split in four corners, and each corner can be assumed to be a separate system as in a quarter car model. (figure 33) This model consists of two suspended masses, i.e., Sprung and Unsprung mass. The tire is considered as an elastic component and is treated as a spring. The Spring and the Damper rates used in this model are assumed to be acting at the wheel center. Thus the installation ratio is considered. Applying Newton's second law to each body, following mathematical models are developed [5], [7], [15].

$$\begin{bmatrix} m_f & 0 \\ 0 & m_{uf} \end{bmatrix} \begin{Bmatrix} \ddot{z}_1 \\ \ddot{z}_2 \end{Bmatrix} + \begin{bmatrix} c_f & -c_f \\ -c_f & c_f \end{bmatrix} \begin{Bmatrix} \dot{z}_1 \\ \dot{z}_2 \end{Bmatrix} + \begin{bmatrix} k_{sf} & -k_{sf} \\ -k_{wf} & k_{sf} + k_t \end{bmatrix} \begin{Bmatrix} z_1 \\ z_2 \end{Bmatrix} = \begin{Bmatrix} 0 \\ k_t * z_r \end{Bmatrix} \sin(\omega t) \quad \ldots (4.47)$$

$$\begin{bmatrix} m_r & 0 \\ 0 & m_{ur} \end{bmatrix} \begin{Bmatrix} \ddot{z}_1 \\ \ddot{z}_2 \end{Bmatrix} + \begin{bmatrix} c_r & -c_r \\ -c_r & c_r \end{bmatrix} \begin{Bmatrix} \dot{z}_1 \\ \dot{z}_2 \end{Bmatrix} + \begin{bmatrix} k_{sr} & -k_{sr} \\ -k_{sr} & k_{sr} + k_t \end{bmatrix} \begin{Bmatrix} z_1 \\ z_2 \end{Bmatrix} = \begin{Bmatrix} 0 \\ k_t * z_r \end{Bmatrix} \sin(\omega t) \quad \ldots (4.48)$$

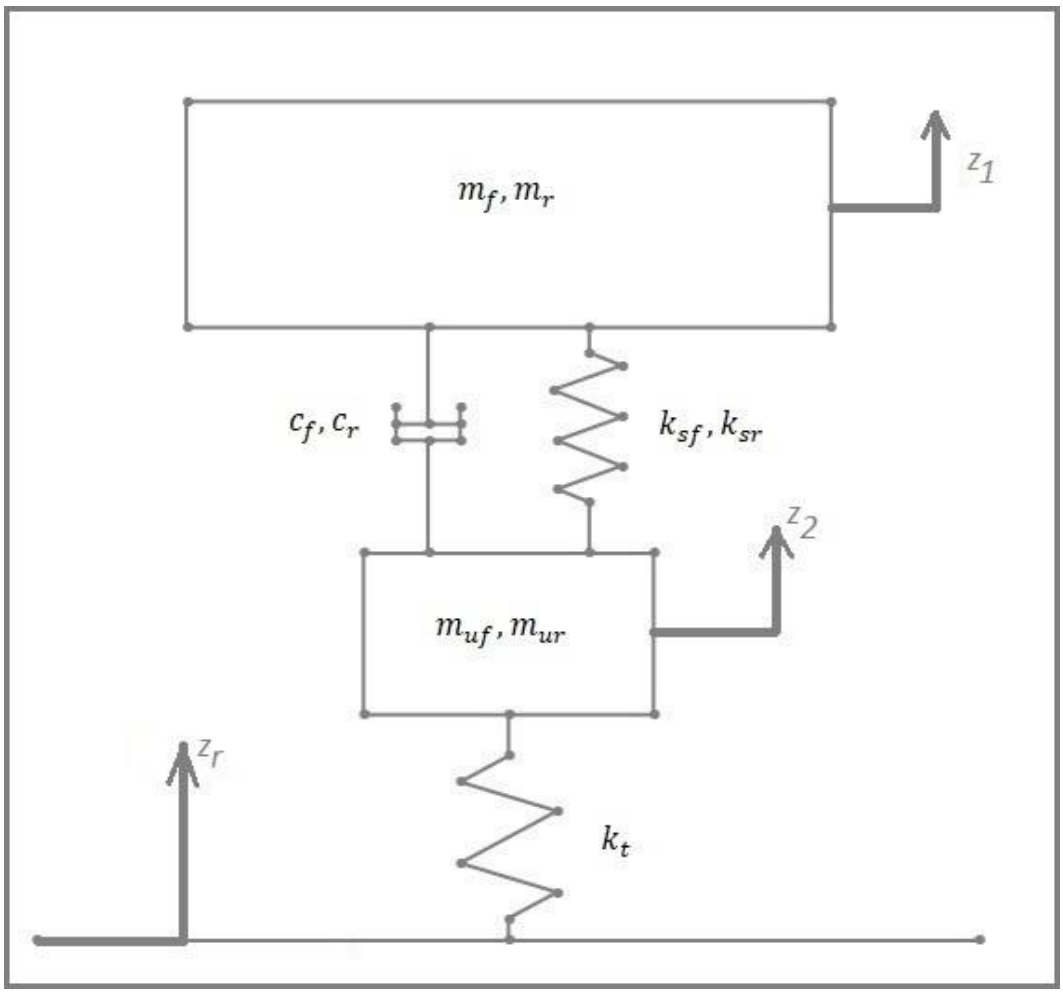

Figure 33. Quarter vehicle model

The models in equations 4.47 and 4.48 are of the form

$$[M][\ddot{z}] + [C][\dot{z}] + [K][z] = \{F\} \tag{4.49}$$

Where, $[M] = \begin{bmatrix} m_f & 0 \\ 0 & m_{uf} \end{bmatrix}$ $[C] = \begin{bmatrix} c_f & -c_f \\ -c_f & c_f \end{bmatrix}$ (4.50a,4.50b)

$[K] = \begin{bmatrix} k_{sf} & -k_{sf} \\ -k_{sf} & k_{sf} + k_t \end{bmatrix}$ $\{F\} = \begin{Bmatrix} 0 \\ k_t * z_r \end{Bmatrix} \sin(\omega t)$ (4.50c, 4.50d)

Assuming particular solution for a forced vibration condition, let

$$\{z_p\} = \{Z\}e^{i\omega t} \quad (4.51a)$$

Then, $$\{\dot{z}_p\} = i\omega\{Z\}e^{i\omega t} \quad (4.51b)$$

And, $$\{\ddot{z}_p\} = -\omega^2\{Z\}e^{i\omega t} \quad (4.51c)$$

From equations 4.49,4.50 and 4.51 we can write,

$$[(K - \omega^2 M) + i\omega C]\{Z\}e^{i\omega t} = \{F\}e^{i\omega t} \quad (4.52)$$

Therefore,

$$\{Z\} = [(K - \omega^2 M) + i\omega C]^{-1}\{F\} \quad (4.53)$$

Parameters: -

Mf = 118.25 kg	Mr = 96.75 kg	
Muf = 10 kg	Mur = 25 kg	
Cf = 1750 Ns/m	Cr = 1750 Ns/m	
Ksf = 22218 N/m	Ksr = 26145 N/m	Kt = 200000 N/m

4.4.1 Results and Discussion

The quarter vehicle transmissibility analysis shows an overall improvement in gen 2.5 vehicle's response than that of Gen 2. As shown in figure 34, the response gain is significantly lowered and the ride frequencies have been reduced as well. The part of this improvement is due to the choice of radial tires instead of bias ply. Which helped reduce the stiffness, also, the dampers used in Gen 2.5 provide higher damping ratio. Gen 2.5 vehicle's rear suspension shows a second peak around 15 Hz because of the heavier unsprung mass due to hub motors. The ride frequencies of the front axle have been brought down below 2Hz which is deemed comfortable for passenger vehicles [5]. However the ride frequency of the rear axles is still little over the desired value (table 7). The response gain of both the suspensions at the natural frequency is close to each other reducing the pitch of the vehicle unlike in Gen 2. (table 8) Overall, the ride quality of Gen 2.5 should be perceived better than that of Gen 2 by the passengers.

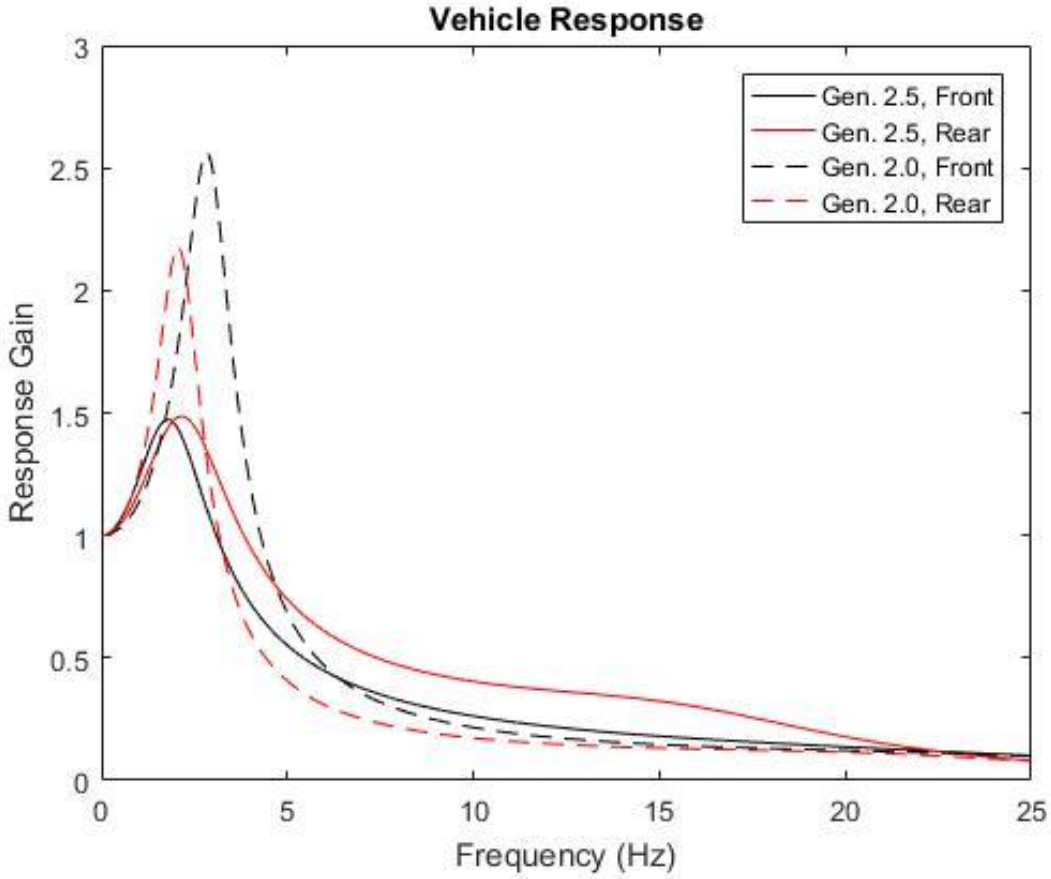

Figure 34. Comparison of suspension isolation behavior of quarter vehicle model between gen 2 and 2.5.

Table 7. Natural Ride Frequencies of the Front and Rear, Gen 2.0 & 2.5

Damped Natural Frequencies	**Gen 2.0**	**Gen 2.5**
Front	2.82 Hz	1.78 Hz
Rear	2.05 Hz	2.15 Hz

Table 8. Response gain of the front and rear suspension of, Gen 2.0 & 2.5

Peak Response Gain	**Gen 2.0**	**Gen 2.5**
Front	2.56	1.47
Rear	2.175	1.49

CHAPTER 5: STABILITY ANALYSIS

This chapter will study the cornering behavior of the vehicle, also known as handling characteristics. The handling of any vehicle is used to imply the vehicle's response behavior to directional or steering input. The most common measure used to quantify a vehicle's directional response is called as 'Understeer Gradient.' It assumes the vehicle negotiating a corner in steady state and a simplified model of the vehicle is used known as 'bicycle model.'

5.1 Bicycle Model

The bicycle model (figure 35) is widely used to study basic handling characteristics. This model has 2 degrees of freedom that consist of yaw 'r' and lateral 'v' velocities. This model neglects any effects due to lateral or longitudinal load transfer, rolling or pitching motions, aerodynamics and suspension compliance. The steering input is given by the steering angle 'δ.'

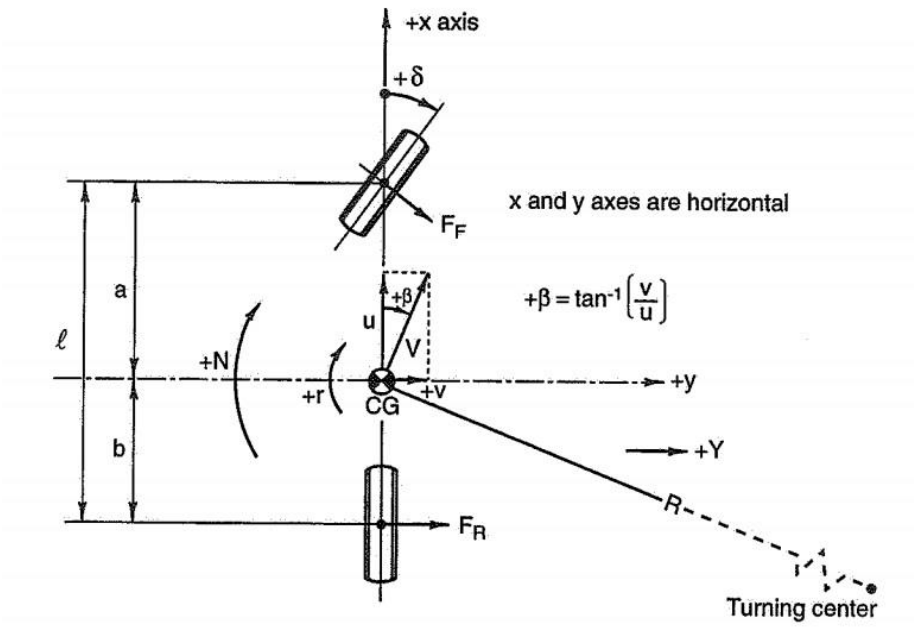

Figure 35. The 2DOF bicycle model.[6]

5.2 Steady State Cornering

In any cornering condition, a vehicle usually goes through three phases. The first one is ‘Corner Entry.’ In this phase, the vehicle is initially traveling in a straight line, i.e., the yaw and lateral velocities are zero. These velocities build up from zero to a certain value and so do the slip angles at the tires. The next phase is steady state cornering, where the lateral and yaw velocities remain constant, and the vehicle turns about with a constant turn radius. The last phase is the ‘Corner Exit’ where the lateral and yaw velocities again drop to zeros and the vehicle travels in a straight line.

To understand the geometry of cornering, consider a vehicle is negotiating a turn at a low speed. As discussed before, there are no dynamic load transfer effects, and the speed is too low to develop any slip angles at the tires. A steering angle ‘δ’ is applied to negotiate a turn of radius ‘R,' known here as the Ackermann steering angle.

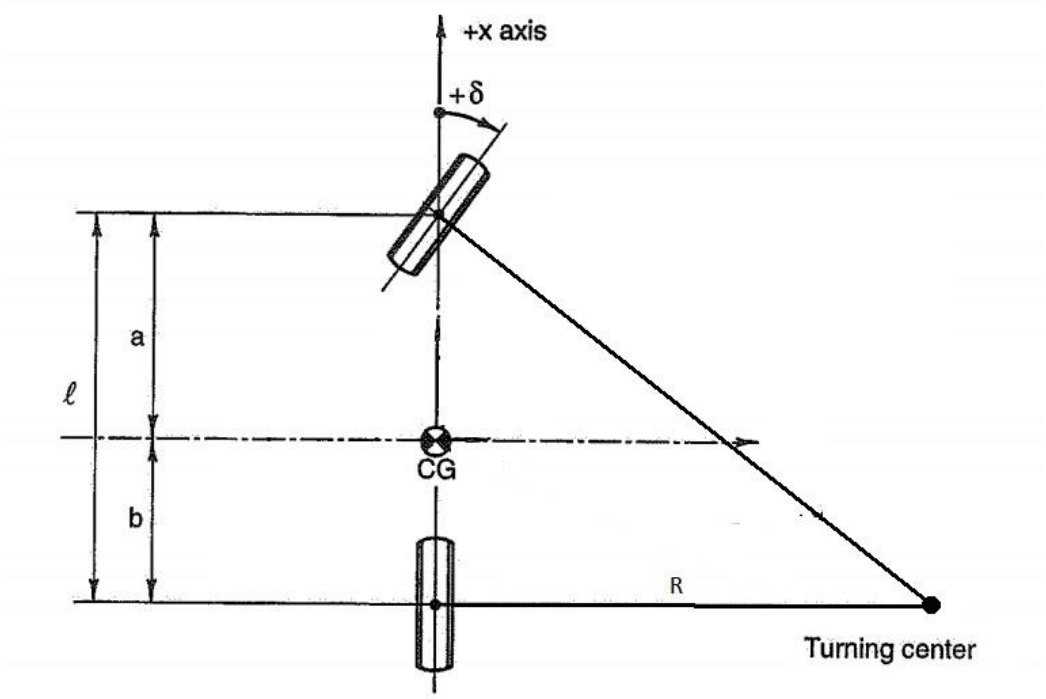

Figure 36. Low-Speed Cornering and Ackermann Steering Angle

The Ackermann Steering angle is given as:

$$\delta = \frac{l}{R} \tag{5.1}$$

At higher speeds, the lateral acceleration increases, and the tires develop slip angles. The slip angle is the angle between a tire's heading direction and the traveling direction. This phenomenon arises due to elastic nature of the rubber tires and the relationship between the slip angle and the lateral force is given by cornering stiffness 'C_α.' Each tire, depending upon its model (build and compound) and the manufacturer, will have a different value for the cornering stiffness. Another way of describing the cornering stiffness is by cornering coefficient 'CC_α.' The relationship between the cornering stiffness and cornering coefficient is

$$C_\alpha = CC_\alpha F_z \tag{5.2}$$

Where, F_z is the vertical load on the tire.

And the slip angle of a tire is

$$\alpha = \frac{F_y}{C_\alpha} \tag{5.3}$$

The cornering stiffness of the tires used in EcoPRT vehicles is not known, thus referring to Gillespie [5] and Dukkipati [7] a typical value is chosen.

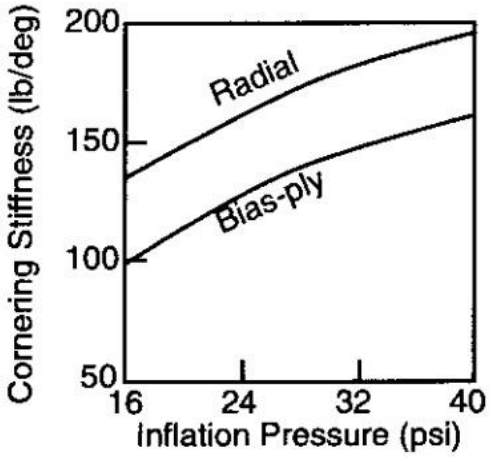

Figure 37. Cornering stiffness for radial and bias plies tires

Both EcoPRT vehicles use the same tires on both axles, also, the CG is placed near the center of the vehicle. Thus the load difference between the front and the rear axle will not significantly change the cornering stiffness.

$C_{\alpha 1}$ = 140 lb/deg = 624.9 N/deg (Gen 2 with bias tires)

$C_{\alpha 2}$ = 180 lb/drg = 803.5 N/deg (Gen 2.5 with radial tires)

5.3 Understeer Gradient

Now, looking at the bicycle model below, considered negotiating a high-speed turn, the wheelbase is much smaller than the turn radius, and thus small angles are assumed. Also, the difference between the steer angles of the left and right front wheels is negligible. A mean steering angle 'δ' is assumed.

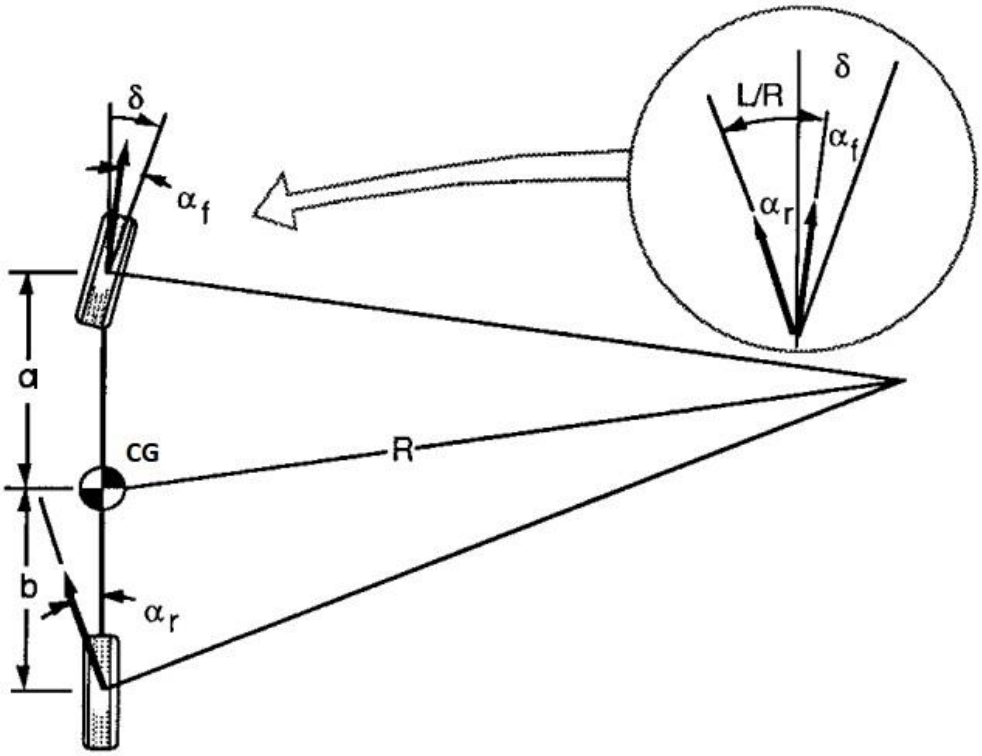

Figure 38. Bicycle model cornering at high speed. [5]

Applying Newton's second law to lateral and rotational motion,

$\Sigma F_y = F_{yf} + F_{yr} = Ma_y$ (5.4) (Lateral forces acting on both axles)

$\Sigma M = F_{yf}\, a - F_{yr}\, b = 0$ (5.5) (Moment acting at CG due to lateral forces)

Where, $a_y = \frac{V^2}{R}$ is lateral acceleration, M is mass of the vehicle, and a and b are the distances of front and rear axles from the CG respectively. Then, equation 5.5 can be rewritten as

$$F_{yf} = F_{yr}\frac{b}{a} \tag{5.6}$$

Substituting in equation. 5.4, we get

$$\frac{MV^2}{R} = F_{yr}\frac{b}{a} + F_{yr}$$

$$F_{yr} = \frac{MaV^2}{lR} \qquad (l = a+b) \tag{5.7}$$

Equation 5.7 indicates that the amount of lateral force generated at the rear axle is proportional to the portion of weight carried by the rear axle. ($Ma/l = W_r/g$) Thus, from the above result and equation 5.3,

$$\alpha_f = \frac{W_f V^2}{C_\alpha g R} \qquad \text{and} \qquad \alpha_r = \frac{W_r V^2}{C_\alpha g R} \tag{5.8}$$

Now, considering the steering geometry and the slip angles from figure 38, we can write

$$\delta = \frac{180}{\pi}\frac{l}{R} + \alpha_f - \alpha_r \qquad \text{(degrees)} \tag{5.9}$$

Therefore, from equation 5.8 and 5.9, we get

$$\delta = \frac{180}{\pi}\frac{l}{R} + \frac{W_f V^2}{C_\alpha g R} - \frac{W_r V^2}{C_\alpha g R}$$

$$\delta = 57.3\frac{l}{R} + \left(\frac{W_f}{C_\alpha} - \frac{W_r}{C_\alpha}\right)\frac{V^2}{gR} \tag{5.10}$$

Which can be rewritten in shorthand as

$$\delta = 57.3\frac{l}{R} + KA_y \tag{5.11}$$

Here, K is known as the understeer gradient. The value of K can be positive or negative determining the magnitude and the change in steering angle input required to negotiate a certain turn. A vehicle with positive K has understeer property, i.e. the steering angle has to be increased with the increase in lateral acceleration while cornering through the same turn and vice versa if the K value is negative. In the latter case, the vehicle has oversteer property.

K for Gen 2 vehicle = -0.8001 deg/g (Oversteer)
K for Gen 2.5 vehicle = 0.6223 deg/g (Understeer)

Consider a cornering condition with a constant radius of 35 m. Then, according to the equation 5.11, the steering angle input and its variation with speed is shown in figure 39.

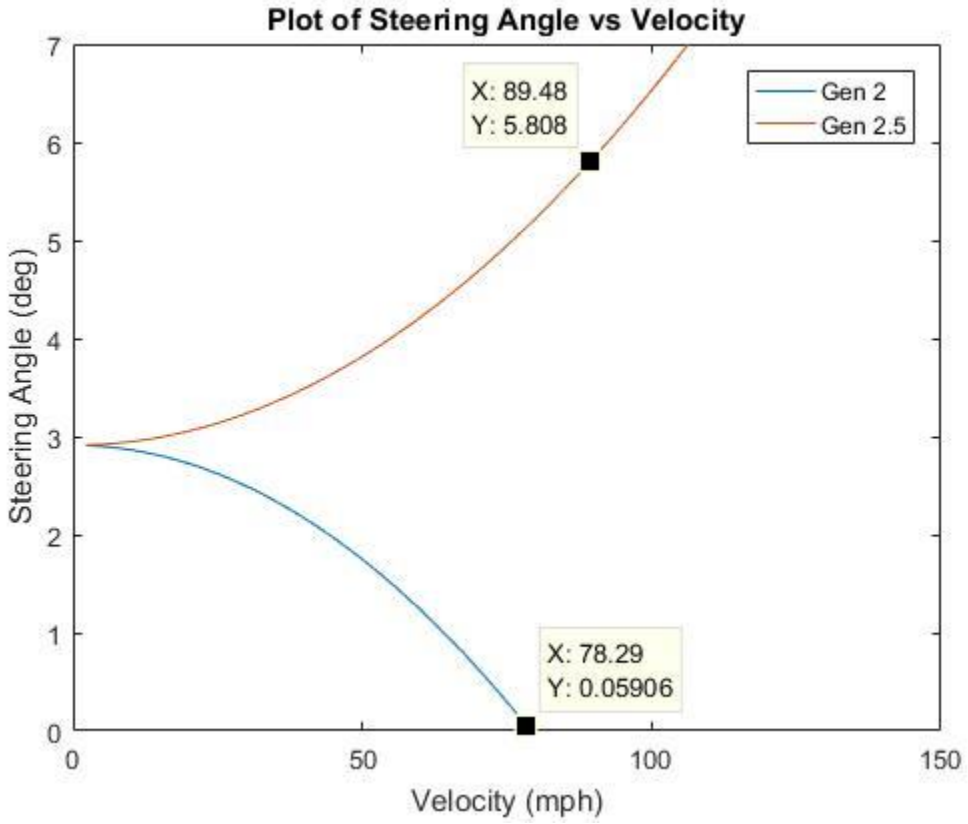

Figure 39. Steering angle input variation of Gen 2 and Gen 2.5 for constant radius turn.

The figure 37 indicates that the gen 2 vehicle oversteers while 2.5 understeers. In this case, the two different characteristics to be defined are the critical speed and characteristic speed. Characteristic speed is defined for understeer vehicles. As vehicle speed increases, so does the steering angle required to negotiate the same turn. The speed at which the steering angle required is twice the static value, is called the characteristic speed. However, for an oversteer vehicle, critical speed is defined as the speed at which the required steering input becomes zero.

From equation 5.11, we can define the characteristic speed as

$$2\ x\ 57.3\frac{L}{R} = \ 57.3\frac{l}{R} + KA_y$$

$$KA_y = 57.3\frac{l}{R}$$

$$\frac{V^2}{gR}K = 57.3\frac{l}{R}$$

$$V_{char} = \sqrt{\frac{57.3\ lg}{K}} \qquad (5.12)$$

And the critical speed

$$0 = \ 57.3\frac{l}{R} + KA_y$$

$$KA_y = -57.3\frac{l}{R}$$

$$\frac{V^2}{gR}K = -57.3\frac{l}{R}$$

$$V_{crit} = \sqrt{-\frac{57.3\ lg}{K}} \qquad (5.13)$$

In the given example, for 35m radius turn, the characteristic speed of Gen 2.5 vehicle is 90mph and the critical speed for Gen 2 is 78mph and the characteristic speed for the Gen 2.5 is 89.5 mph. It is highly unlikely that any of these vehicles will ever be driven at these speeds. Note that the understeer vehicle will never be unstable, but this study assumes no aerodynamic effects or any kind of road disturbances that naturally are omnipresent.

5.3.1 Lateral Acceleration Gain

The effects of understeer gradient can be observed by plotting response of the vehicle to steering inputs for varying speed. This response is usually measured in lateral acceleration or the yaw rate. [5]–[7], [16] Either of these could be more important than the other depending upon a given situation. In case of changing the lane, the change in lateral acceleration is more important than the change in heading and considering case of right-hand turn at a junction, change of heading is more important than lateral acceleration, However the relationship between the two is of the form "cause and effect." The lateral acceleration gain is the rate of increment of acceleration per unit steer angle increment and the relationship is derived from equation 5.11. The response of Gen 2 and 2.5 is shown in figure 38.

$$\frac{A_y}{\delta} = \frac{\frac{V^2}{gR}}{57.3\frac{l}{R}+KA_y} = \frac{\frac{V^2}{57.3\ gl}}{1+\left(K\frac{V^2}{57.3\ gl}\right)} \tag{5.14}$$

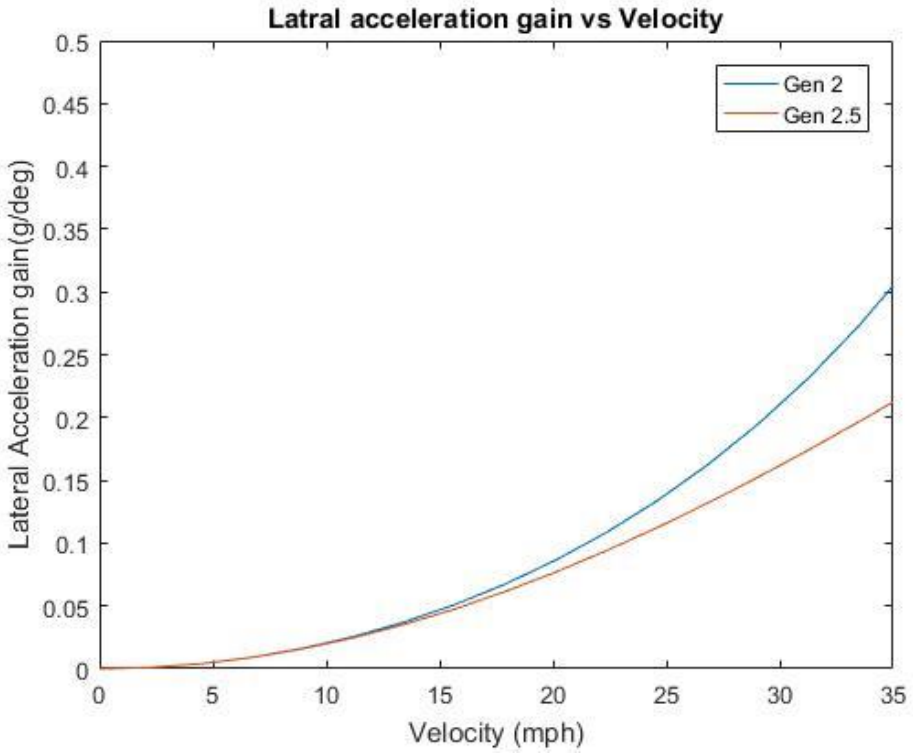

Figure 40. Lateral acceleration gains of Gen 2 and Gen 2.5 vehicles for increasing speed

5.3.2 Yaw Velocity Gain

Yaw rate gain is the increase in yaw rate of the vehicle per degree of steering input. Figure 39 shows the response of Gen 2 and 2.5 to the steering input at varying speeds. The yaw rate gain for the oversteering gen 2 gradually increasing with increasing slope, at the critical speed this rate becomes infinite, while in case of understeering Gen 2.5, although the yaw rate increases gradually, it reaches the maximum value at its characteristic speed and reduces further after. The yaw rate per degree of steering input is given as follows

$$\frac{r}{\delta} = \frac{\frac{57.3\,V}{R}}{57.3\frac{l}{R}+KA_y} = \frac{\frac{V}{l}}{1+\left(K\frac{V^2}{57.3\,gl}\right)} \tag{5.15}$$

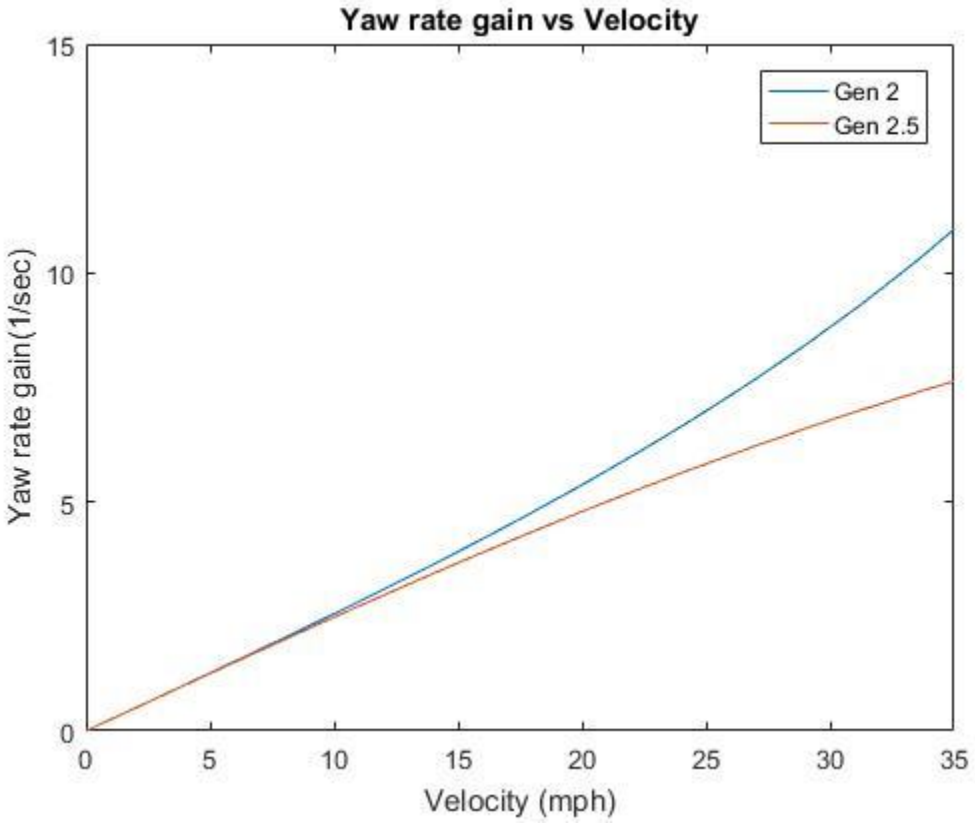

Figure 41. Yaw rate gain of Gen 2 and Gen 2.5 vehicles for increasing speed

5.4 Other Contributions to the Understeer Gradient

As discussed in above sections, the understeer gradient determines the change in the steering angle required to maintain a certain constant radius cornering condition. However, the above section only discusses the effect of physical parameters on the gradient such as the weight distribution and the cornering stiffness of tires on each axle. In case of independent suspension, the kinematic parameters affect the steering angle on the wheels and thus need to be accounted for while considering the overall understeer gradient. The understeer gradient deals with the lateral/yaw motion of the vehicle, i.e. any motions that induce body roll. Thus, the kinematic steering compliance due to body roll/lateral acceleration needs to be accounted for.

The overall understeer gradient is given by[5]–[7], [16], [17]

$$K = K_{tire} + K_{rollstr} + K_{rollcam} + K_{altorque} + K_{steercomp} + K_{lfc} + K_{llt} \quad (5.16)$$

Where,

K_{tire} is due to cornering stiffness of the tires on each axle and the weight distribution, where W_f and W_r are front and rear weight distributions respectively, and C_α is cornering stiffness of the respective tires. It is given by

$$K_{tire} = \frac{W_f}{C_{\alpha f}} - \frac{W_r}{C_{\alpha r}} \quad (5.17)$$

$K_{altorque}$ is due to the aligning torque acting at the wheels, where N_α is the aligning torque coefficient of the respective tires. It is given by

$$K_{altorque} = \frac{W_f}{C_{\alpha f}} \frac{N_{\alpha r}}{bC_{\alpha r}} - \frac{W_r}{C_{\alpha r}} \frac{N_{\alpha f}}{aC_{\alpha f}} \quad (5.18)$$

$K_{steercomp}$ is due to aligning torque deflection steer, where E_α is deflection steer coefficient due to aligning torque and is given by

$$K_{steercomp} = \frac{W_f}{C_{\alpha f}} \frac{N_{\alpha r}}{bC_{\alpha r}} (1 + E_{af} N_{\alpha f}) - \frac{W_r}{C_{\alpha r}} \frac{N_{\alpha f}}{aC_{\alpha f}} (1 - E_{ar} N_{\alpha r}) \qquad (5.19)$$

K_{lfc} is due the the lateral force compliance steer effect where E_f is deflection steer coefficient due to lateral force and is given by

$$K_{lfc} = E_{ff} \frac{W_{sf}}{2} + E_{fr} \frac{W_{sr}}{2} \qquad (5.20)$$

$K_{rollstr}$ is the change in steering angle of the wheels due to the body roll, where K_Φ' is roll gradient and ε is roll steer gradient and is given by.

$$K_{rollstr} = K_\varphi' (\varepsilon_f + \varepsilon_r) \qquad (5.21)$$

$K_{rollcam}$ is due to the camber change at the wheels due to body roll, where C_γ is camber stiffness of the tires and Γ is the roll camber gradient and is given by

$$K_{rollcam} = K_\varphi' \left(\frac{C_{\gamma f} \Gamma_f}{C_{\alpha f}} - \frac{C_{\gamma r} \Gamma_r}{C_{\alpha r}} \right) \qquad (5.22)$$

Lastly, K_{llt} is due to the lateral load transfer and roll camber and is given by

$$K_{llt} = K_\varphi' \left(\frac{C_{\gamma f} \Gamma_f}{C_{\alpha f}} E_{af} N_{\alpha f} - \frac{C_{\gamma r} \Gamma_r}{C_{\alpha r}} E_{af} N_{\alpha f} \right) \qquad (5.23)$$

The combined equation for the understeer gradient is given by

$$K = \frac{W_f}{C_{\alpha f}}\left(1 + \frac{N_{\alpha r}}{bC_{\alpha r}}\right)\left(1 + E_{af}N_{\alpha f}\right) - \frac{W_r}{C_{\alpha r}}\left(1 - \frac{N_{\alpha f}}{aC_{\alpha f}}\right)\left(1 - E_{afr}N_{\alpha r}\right) + E_{ff}\frac{W_{sf}}{2} + \cdots$$
$$\ldots + E_{fr}\frac{W_{sr}}{2} + K_{\varphi}\left(\frac{C_{\gamma f}\Gamma_f}{C_{\alpha f}}(1 + E_{af}N_{\alpha f}) - \frac{C_{\gamma r}\Gamma_r}{C_{\alpha r}}(1 - E_{af}N_{\alpha f}) + \varepsilon_f + \varepsilon_r\right) \quad (5.24)$$

In the equation given above the known parameters are obtained from the kinematic analysis performed in chapter 3. They are as given in table below.

Table 9. Known kinematic and physical parameters for Gen 2.5 vehicle.

Parameter	Value	Parameter	Value
W_f	1375 N	Γ_f	6.2 deg/g
W_r	1125 N	Γ_r	6.2 deg/g
a	0.8	ε_f	-0.156 deg/g
b	0.978	ε_r	0 deg/g
K_Φ	8.05 deg/g		

CHAPTER 6: FUTURE WORK

6.1 Understeer Gradient

The understeer gradient, as discussed in the last chapter, is influenced by various tire parameters. A detailed tire model with cornering stiffness, camber stiffness, aligning torque coefficient and deflection steer coefficient values need to be developed. Otherwise, the road tests can be performed according to the SAE standard J266 to determine the overall understeer gradient of the vehicle. This test includes two test procedures. One with constant radius turn and varying speeds and the other with constant speed and varying turning radius.

6.2 Transient Analysis

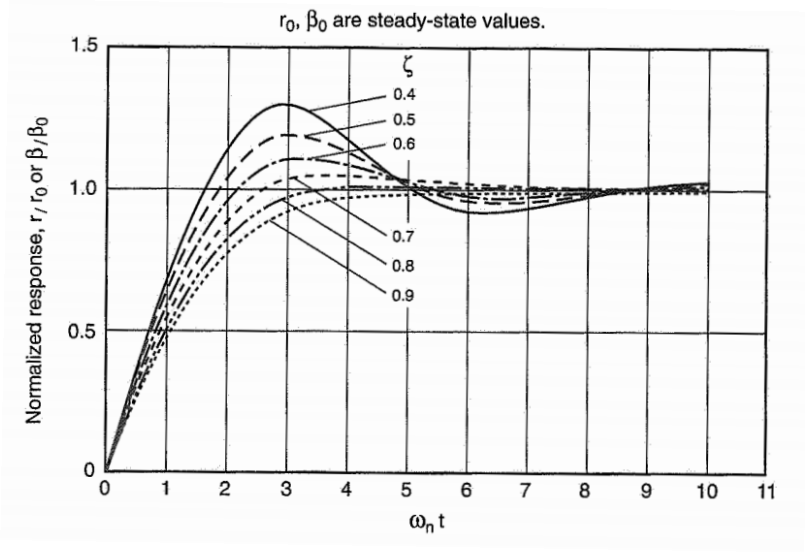

Figure 42. System response for step steer input [6].

A generic bicycle model, can be written in terms of the Laplace operator, transfer function relationships can be obtained for the input and output of steering angle δ and yaw rate r, respectively. The transient response analysis will provide further insights on the stability and the disturbance control of the vehicle

6.3 Dynamic Bicycle Model

A simulator interface has been developed by the team to test the control and path planning algorithm of the vehicle. The simulator currently utilizes a kinematic bicycle model. With the help of the physical and kinematic parameters developed in this study and the road tests, a dynamic model can be built, which will predict near accurate behavior of the vehicle.

REFERENCES

[1] R. Wallace, A. Stentz, C. E. Thorpe, H. Moravec, W. Whittaker, and T. Kanade, "First Results in Robot Road-Following.," *Ijcai*, pp. 1089–1095, 1985.

[2] SAE international, "AUTOMATED DRIVING - LEVELS OF DRIVING AUTOMATION ARE DEFINED IN NEW SAE INTERNATIONAL STANDARD J3016," *SAE Int.*, p. 1, 2016.

[3] I. of the C. HDR Engineering, "2012 CAMPUS MOBILITY PLAN FINAL REPORT," 2012.

[4] S. Hollar *et al.*, "A New Low Cost, Efficient, Self-Driving Personal Rapid Transit System," *IEEE Intell. Veh.*, 2017.

[5] T. D. Gillespie, *Fundamentals of Vehicle Dynamics*. Warrendale, PA: Society of Automotive Engineers, Inc., 1992.

[6] W. F. Milliken and D. L. Milliken, *Race Car Vehicle Dynamics*. Warrendale, PA: SAE International, 1995.

[7] R. Dukkipati, J. Pang, M. Quatu, G. Sheng, and Z. Shuguang, *Road Vehicle Dynamics*. Warrendale, PA: SAE International, 2008.

[8] J. Dixon, *Suspension Analysis and Computational Geometry*, 1st ed. John Wiley & Sons, Ltd, 2009.

[9] C. Smith, *Tune to Win*. Fallbrook, CA: Aero Publishers, 1978.

[10] S. Uberti, M. Gadola, D. Chindamo, M. Romano, and F. Galli, "Design of a double wishbone front suspension for an orchard-vineyard tractor: Kinematic analysis," *J.*

Terramechanics, vol. 57, pp. 23–39, 2015.

[11] J. Hinch, S. Shadle, and K. TM, "NHTSA's rollover rulemaking program -- Results of testing and analysis," *SAE Int.*, vol. 920581, pp. 109–122, 1992.

[12] A. S. Tomar, "Estimation of Steady State Rollover Threshold for High Capacity Transport Vehicles using RCV Calculation Method Master ' s thesis in Automotive Engineering Department of Applied Mechanics," 2015.

[13] M. Giaraffa, "Tech Tip : Springs & Dampers, Part One." [Online]. Available: http://www.optimumg.com/docs/Springs%26Dampers_Tech_Tip_1.pdf.

[14] D. Seward, *Race Car Design*. New York: Palgrave Macmillan, 2015.

[15] S. Hegazy and C. Sandu, "Vehicle Ride Comfort and Stability Performance Evaluation," *SAE Tech. Pap. Ser.*, vol. 4970, 2009.

[16] R. Bundorf, "The influence of vehicle design parameters on characteristic speed and understeer," *SAE Tech. Pap. Ser.*, vol. 1, 1967.

[17] N. R. Dixit, "Evaluation of Vehicle Understeer Gradient Definitions," Ohio State University, 2009.

APPENDICES

A1. EcoPRT prototype vehicle spec-sheet for Gen 2.5.

	Front	Rear
Dimensions		
Overall Length, Width, Height	2297.2 mm ; 870 mm ; 1943.5 mm	
Wheelbase	1.778 m	
Trackwidth	0.771 m	0.771 m
Curb weight	250 Kg	
Gross weight	500 Kg	
Suspension		
Suspension type	SLA, outboard Coilover	SLA, outboard Coilover
Tires	R 10 3.5/90	R 10 3.5/90
Wheels	10 x 3	10 x 3
CG Height	620 mm	
Wheel travel	±50.8 mm	±50.8 mm
Wheel rate	22218 N/m	26465 N/m
Roll rate	8.04 deg/g	
Sprung mass natural frequency	1.78 Hz	2.14 Hz
Damping constant	1750 Ns/m	1750 Ns/m
Motion ratio	0.52	0.49
Static Camber	0 deg	0 deg
Caster	8 deg	8 deg
KPI	5 deg	5 deg
Static Ackermann	50%	
Geometric RC	80 mm	75 mm
Brakes/Hubs		
Rotors	Outboard 7” dia. SS vented	Outboard 7” dia. SS vented
Master Cylinders	Wilwood 260-5520 ½” bore	Wilwood 260-5520 ½” bore
Calipers	Wilwood PS1 1” dia. floating	Wilwood PS1 1” dia. floating
Hub Bearings	Double tapered roller bearings	N/A
Knuckle/Upright	7075 T6 Single block CNC	7075 T6 Single block CNC
Frame		
Frame construction	Space Frame	
Material(s)	AISI 1018/1020/4130, Al 6061/6063	
Torsional stiffness	800 Nm/deg	
Frame weight	60 Kg	
Safety	Roll cage, Side impact structure	
Body	Thermoformed ABS	
Powertrain		
Motor	N/A	2x 4kW 72V BLDC Hub motors
Battery pack	2x 36V Li-Mn Batteries	

A2. EcoPRT Gen 2.5 Vehicle Design

A2.1 Overview of the systems

Figure 43. Overview of the mechanical and perception system in an EcoPRT Vehicle.

Note: Dr. Seth Hollar is also affiliated with WISER Systems

A2.2 Mechanical Design

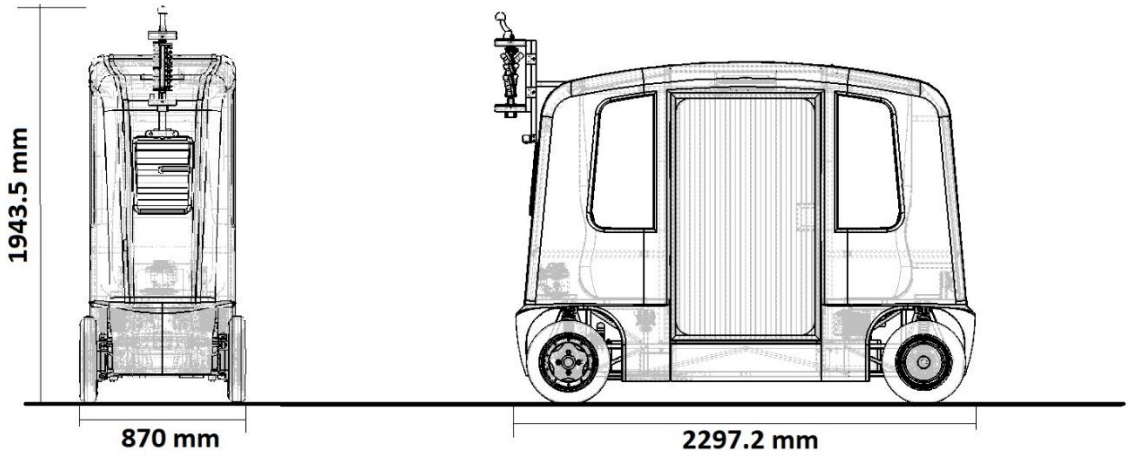

Figure 44. Overall dimensions of Gen 2.5 Vehicle.

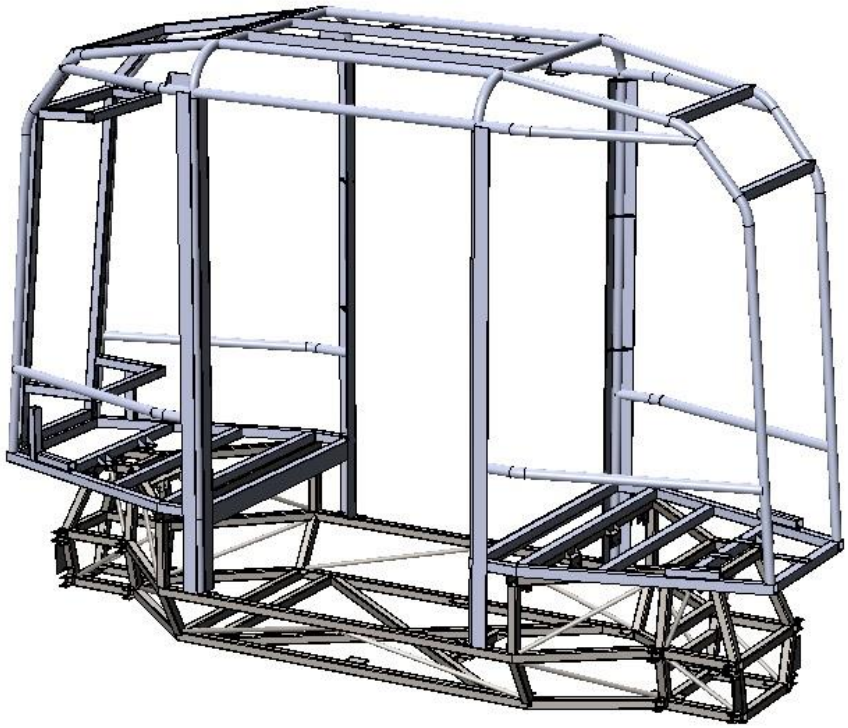

Figure 45. Steel and Aluminum space frame construction with side impact and roll structure.

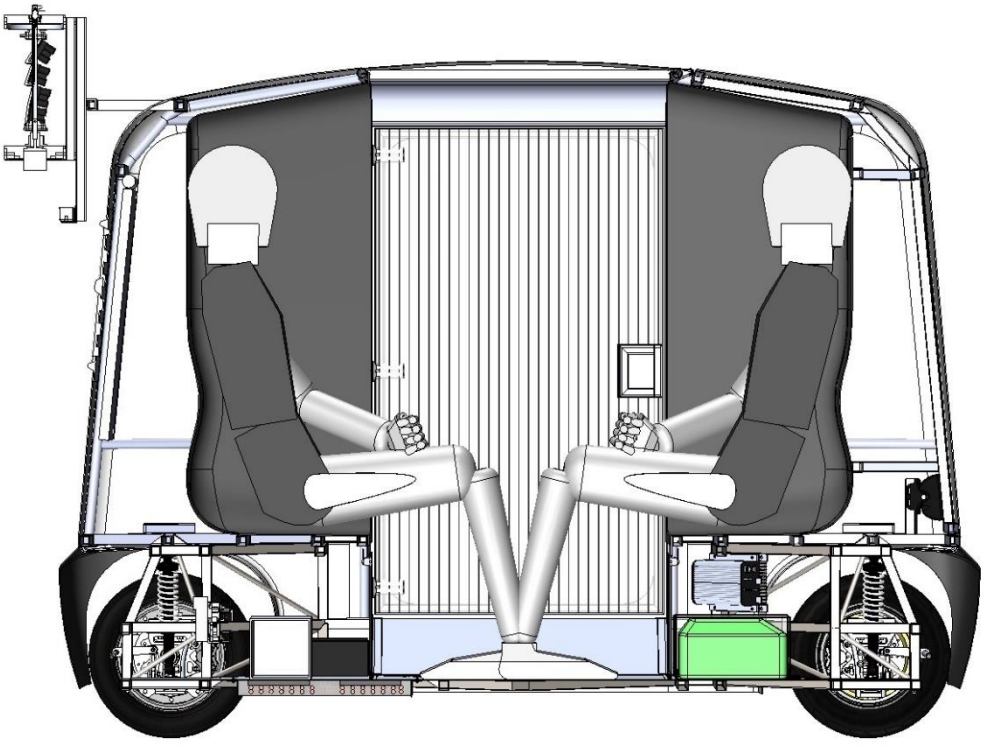

Figure 46. Gen 2.5 section view with two 95th percentile male passengers.

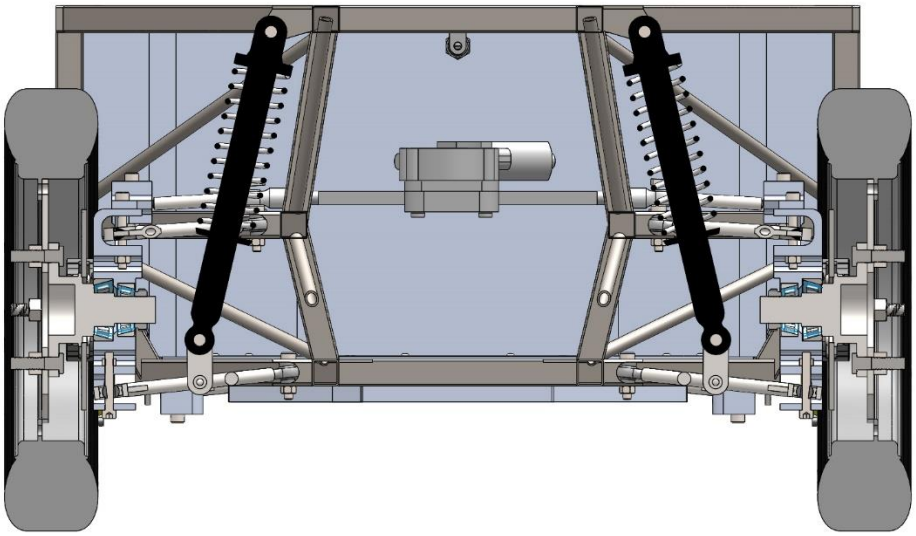

Figure 47. Gen 2.5 front suspension section view.

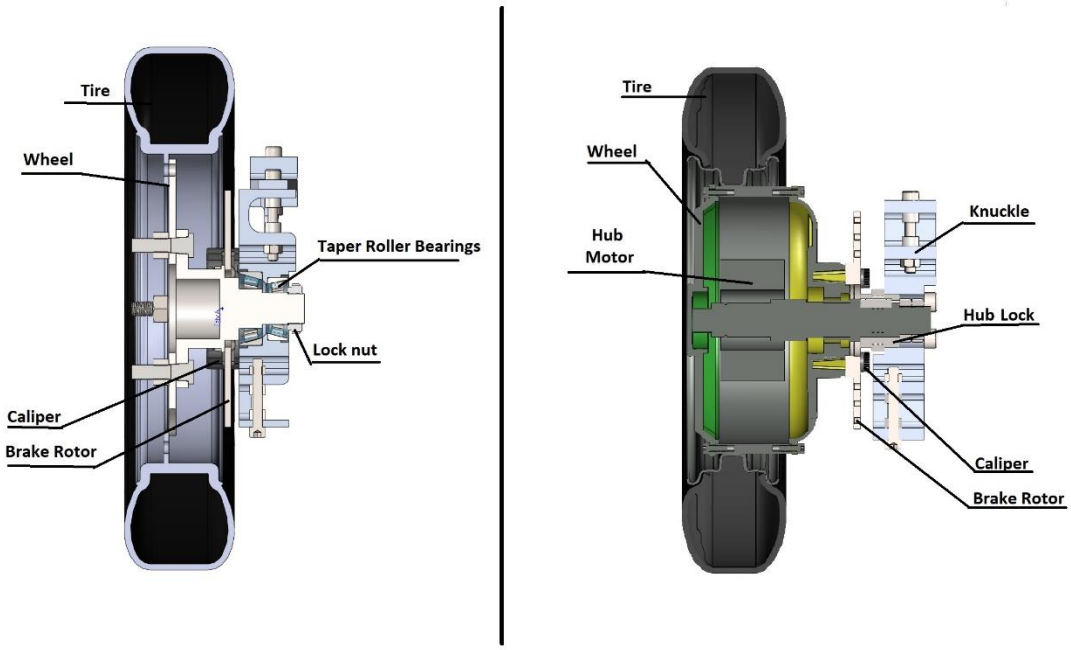

Figure 48. Gen 2.5 front and rear wheel assembly components.

A3 Lateral Load Transfer

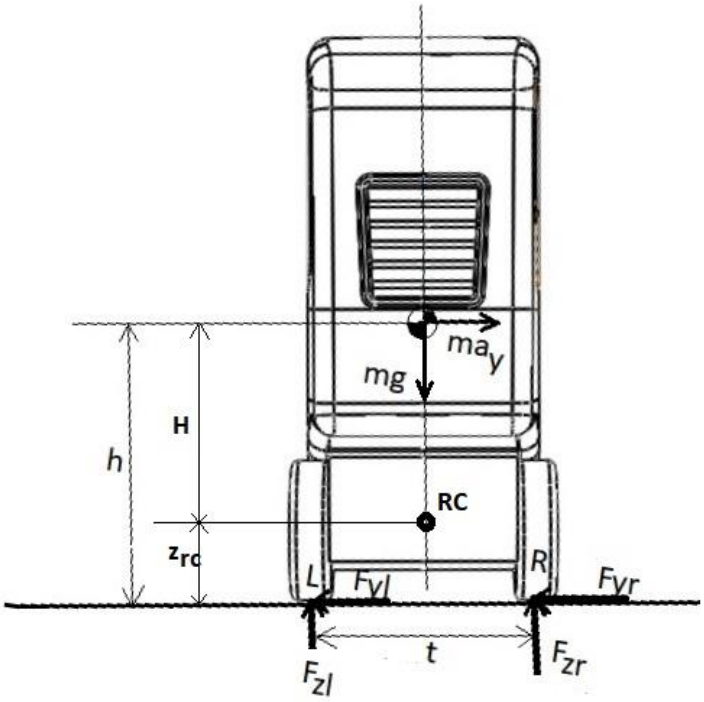

Figure 49. Steady state cornering condition

In this analysis, the lateral load transfer for a single axle is calculated. The vehicle is assumed to be cornering around a turn with constant velocity and turn radius, i.e. steady state (Figure 46). If a weight transfer of ΔW is considered over a track width of t, the generic moment is given by

$$M = \Delta W t \qquad \text{or} \qquad \Delta W = \frac{M}{t} \qquad \text{(A3.1)}$$

Thus, the load transfer caused by any moment M is the moment divided by the track width. There are three components of moment acting towards the weigh transfer. First, the moment due to unsprung weight (M_u), then the kinematic load transfer moment due to the sprung and Unsprung weight connection at the roll center (M_k) and lastly, the elastic roll moment – due to the suspension compliance and/or body roll (M_s). These moments can be

considered individually and then combined to find the total load transfer by the law of superposition.

Now for the front axle, the unsprung weight is W_{uf} and the CG of isolated front suspension is located at a height h_{uf}. Thus, due to the lateral acceleration Ay, the moment due to unsprung weight is

$$M_u = W_{uf} A_y h_{uf} \quad \text{(A3.2)}$$

Moreover, the weight transfer $$\Delta W_u = \frac{W_{uf} A_y h_{uf}}{t} \quad \text{(A3.3)}$$

Now, the kinematic weight transfer due to the connection between the sprung and unsprung mass. As the lateral force acts on the sprung mass, the inertial force acts at the roll center due to the unsprung mass. Which is the force coupling between the sprung and unsprung mass.

$$M_k = W_{sf} A_y z_{rcf} \quad \text{(A3.4)}$$

Moreover, the weight transfer $$\Delta W_k = \frac{W_{sf} A_y z_{rcf}}{t} \quad \text{(A3.5)}$$

Moreover, lastly, for the elastic moment component, consider figure 47. The lateral acceleration causes the body roll by an angle Φ. The suspension springs resist this roll by providing roll stiffness equal to KΦf + KΦr. Also, another component of body roll is the moment caused by the shift of CG opposite to the turning direction.

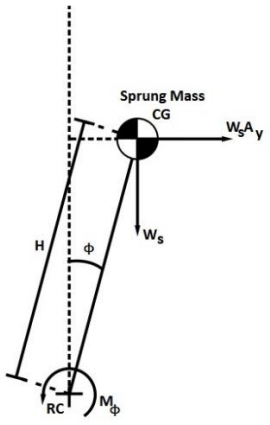

Figure 50. Body roll about the roll center

Thus, the elastic moment has two components to itself, which are,

$$M_s = M_\varphi - M_{CG}$$

$$M_s = K_{\varphi f}\varphi - W_{sf}Hsin(\varphi) \quad \text{(A3.6)}$$

Moreover, the weight transfer, $\Delta W_s = \frac{K_{\varphi f}\varphi - W_{sf}Hsin(\varphi)}{t}$

$$\Delta W_s = \frac{K_{\varphi f}\varphi - W_{sf}H\varphi}{t} \quad \text{(A3.7)}$$

Thus, the total load transfer is given by combining equations A3.3, A3.5 and A3.7

$$\Delta W = \Delta W_u + \Delta W_k + \Delta W_s$$

$$\Delta W_f = \frac{W_{uf}A_y h_{uf}}{t} + \frac{W_{sf}A_y z_{rcf}}{t} + \frac{K_{\varphi f}\varphi - W_{sf}H\varphi}{t} \quad \text{(A3.8)}$$

The above equation can be simplified by substituting the expression for roll angle. To find the body roll, consider the figure 47 with combined sprung weight. For the steady state, considering moments acting the roll center,

$$\Sigma M_{RC} = M\varphi = M_s gH\ sin(\varphi) + M_s a_y H\ cos(\varphi)$$

i.e. $$(K_{\varphi f} + K_{\varphi r})\varphi = M_s gH\ sin(\varphi) + M_s a_y H\ cos(\varphi)$$

i.e $$(K_{\varphi f} + K_{\varphi r})\varphi = M_s gH\varphi + M_s a_y H \quad \text{(A3.9)}$$

The above equation can be rewritten to find the roll angle Φ as

$$\varphi = \frac{W_s H A_y}{K_{\varphi f} + K_{\varphi r} - W_s H} \qquad \text{(W=mg; A=a/g))} \quad \text{(A3.10)}$$

Substituting equation A3.10 into A3.8, we get

$$\Delta W_f = \frac{W_{uf}A_y h_{uf}}{t} + \frac{W_{sf}A_y z_{rcf}}{t} + \frac{W_s H A_y}{K_{\varphi f} + K_{\varphi r} - W_s H}\frac{K_{\varphi f} - W_{sf}H}{t}$$

$$\Delta W_f = \frac{W_s A_y}{t}\left(\frac{HK_{\varphi f} - \frac{b}{l}HW_s}{K_{\varphi f} + K_{\varphi r} - W_s H} + \frac{bz_{rcf}}{l}\right) + \frac{W_{uf}A_y h_{uf}}{t} \quad \text{(A3.11)}$$

As described in Milliken the approximate form of equation A3.11 is given by considering the following assumptions.

$$W_u \approx 0$$

$$W_s \approx W$$

$$K_{\varphi f} - \frac{a}{l} W_s \approx K_{\varphi f}$$

$$\Delta W_f = \frac{W_s A_y}{t}\left(\frac{H K_{\varphi f}}{K_{\varphi f} + K_{\varphi r}} + \frac{b z_{rcf}}{l}\right) \quad \text{(A3.12)}$$

Similarly,

$$\Delta W_r = \frac{W_s A_y}{t}\left(\frac{H K_{\varphi r}}{K_{\varphi f} + K_{\varphi r}} + \frac{a z_{rcr}}{l}\right) \quad \text{(A3.13)}$$

Comparing the values obtained for the weight transfer by exact (A3.11) and approximate (A3.12, A3.13) formulae, it can be seen below for 0.5g of lateral acceleration (A_y).

Axle	Exact	Approximate	Error %
ΔWf	1001.5 N	942.1 N	- 5.9%